Fritz Laboratory Reports   Civil and Environmental Engineering

1970

Behavior of structural subassemblages with laterally unsupported columns, June 1970

L.C. Lim

L.-W. Lu

LEHIGH UNIVERSITY

Design of Laterally Unsupported Columns

BEHAVIOR OF STRUCTURAL SUBASSEMBLAGES WITH LATERALLY UNSUPPORTED COLUMNS

by

Lee C. Lim

Le-Wu Lu

Fritz Engineering Laboratory Report No. 329.3

Design of Laterally Unsupported Columns

BEHAVIOR OF STRUCTURAL SUBASSEMBLAGES WITH
LATERALLY UNSUPPORTED COLUMNS

by

Lee C. Lim

Le-Wu Lu

Fritz Engineering Laboratory

Lehigh University

Bethlehem, Pennsylvania

June, 1970

TABLE OF CONTENTS

ABSTRACT

Results are given for tests on two full-size non-sway structural subassemblages with laterally unsupported columns. All columns were designed with the procedure currently recommended for plastically designed structures. The results indicate a substantial post-buckling strength for unbraced columns in a continuous frame system and demonstrate the conservativeness of the current design procedure for this type of column.

1. INTRODUCTION

1.1 Laterally Unsupported Column

In the plastic method of design of planar multi-story frames, columns are assumed to be subjected only to axial load and strong axis bending moments and that out-of-plane deformation is prevented by lateral bracing.[1,2] If, on the other hand, no bracing is provided to the column because of architectural requirements or of economical reason, the column may fail before its full in-plane capacity is reached by lateral-torsional buckling--a type of buckling involving twisting and out-of-plane deformation. This type of column is known as laterally unsupported column.

Lateral-torsional buckling can thus affect the behavior of a laterally unsupported column in two ways:

1. The maximum in-plane moment capacity of the column may not be realized.

2. The rotation capacity may be impaired.

To avoid this type of failure occurring in building frames, it has been recommended that laterally unsupported columns be designed on the basis of a critical moment M_{cr} which is always less than the maximum in-plane moment capacity.[1,3] A commonly used formula for determining the critical moment is the CRC interaction formula.

$$\frac{P}{P_o} + \frac{C_m M_{cr}}{M_o} \left[\frac{1}{1 - \frac{P}{P_e}} \right] \leq 1.0 \qquad (1)$$

In the above equation, P is the applied axial load and is a known quantity in design. The quantity P_o is the maximum axial load that the column can support if no bending moment is present and can be calculated from the expression

$$P_o = P_y \left[1 - \frac{\sigma_y}{4\pi^2 E} \left(\frac{h}{r_y}\right)^2 \right] \tag{2}$$

in which P_y is the yield load of the column, σ_y the yield stress, and E the elastic modulus. The load P_e is the elastic buckling load in the plane of bending and is equal to

$$P_e = \frac{\pi^2 E I_x}{h^2} . \tag{3}$$

in which I_x is the moment of inertia about the strong axis.

The quantity M_o is the maximum bending moment which the column can sustain if no axial force is present. It is dependent on the column slenderness ratio h/r_y and its relationship is given in Ref. 1. The end-moment correction factor C_m is given by

$$C_m = 0.6 - 0.4 q \tag{4}$$

in which q is the ratio of the smaller end moment to the larger end moment and lies between -1 and +1. For a beam-column bent into single curvature by equal but opposite end moments, the value of q is -1. Whereas for the case where only one end moment is applied, q is equal to zero.

Tests on pinned-end and restrained beam-columns report in Refs. 4 and 5 demonstrate the validity of the CRC formula in estimating

the strength of an unbraced column. These tests as well as those reported in Ref. 6 show that the reduction in rotation capacity due to lateral-torsional buckling appears to be greater for more slender columns.

1.2 Subassemblages with Laterally Unsupported Columns

The subassemblage in Fig. 1a is provided to illustrate the concept currently recommended for the design of laterally unsupported columns in a building frame. This subassemblage consists of two columns and an uniformly loaded beam. A constant axial load P is applied on the upper column. The far ends of all member components are assumed pinned. Figure 1b shows schematically the moment-rotation relationships for the upper column, the lower column, and the joint. The latter is obtained by compounding the moment-rotation relationships of the upper and the lower columns. The solid curves thus demonstrate the in-plane response of each column to the end moment transmitted from the beam. The axial load on the upper column is constant during the loading history. However, on the lower column it increases as the uniformly distributed load W is increased. For design simplicity, it is customarily assumed that this axial load is also constant and is equal to the applied axial load P plus the internal reaction at the joint corresponding to the formation of beam mechanism. The quantity M_m denotes the maximum resisting capacity of the joint if the subassemblage exhibits only in-plane deformation.

Because the columns are laterally unsupported, it is necessary to check whether lateral-torsional buckling would occur before M_m is reached. Since no procedure is currently available for calculating

the critical combination of load and moment associated with lateral-torsional buckling of a continuous beam-column, reliance must be made on the procedure for the single column case as given by the CRC formula. As discussed earlier, the critical moment for lateral-torsional buckling of a beam-column depends on the magnitude of the axial load, the end moment ratio, and the slenderness ratio h/r_y. Thus for columns with identical slenderness and end-moment ratios, the critical moment is smaller for the column compressed by higher axial load. For the two columns in Fig. 1a, it is apparent from the previous discussion that lateral-torsional buckling would first occur in the lower column. Suppose that the critical moments M_{cr} for the two columns are as marked on the top two M-θ curves of Fig. 1b, the design moment M_T for the joint, taking into account the possibility of lateral-torsional buckling, is conservatively estimated as that moment corresponding to a rotation equal to the critical rotation θ_{cr} of the lower column. Therefore, considering the possibility of lateral-torsional buckling, the design value for joint moment capacity could be substantially reduced.

1.3 Objectives of Tests

Columns in multi-story frames are usually designed as continuous members. The procedure discussed previously may not be accurate in predicting the strength of a group of columns. Experiments on restrained unbraced columns reported in Refs. 5 and 6 did not provide an answer as to what might be the degree of restraint from the adjacent columns which are not so severely loaded to the column under consideration. Furthermore, the restraints at the joints provided by the floor beams may be substantial enough to prevent the early occurrence of lateral-torsional buckling. In classical theory, bifurcation is a simultaneous

phenomenon for a system consisting of a group of structural members.
The objective of the proposed tests is threefold:

    1. To investigate whether current design procedure for laterally unsupported columns is satisfactory.

    2. To study the strength and behavior of structural sub-assemblages with a number of continuous columns, laterally unbraced between joints.

    3. To observe the failure modes of the continuous columns.

2. TEST SPECIMENS AND TESTING TECHNIQUES

The selection and design of the two subassemblages, the techniques employed in testing these specimens and the methods of data acquisition have been described in considerable detail in Ref. 7. In this report, only a brief summary of the above aspects of the tests is given.

2.1 Description of Test Specimens

The two subassemblages designed are typical interior sub-assemblages of a building frame. Each subassemblage was made up of three columns of equal height and two beams; one framing into the upper joint and the other into the lower joint as shown in Fig. 2. The column height and the spans of the upper and the lower beams were identical for both specimens. The columns height was 10'-2 3/8"; the upper beam spanned 20'-0" and the lower beam 17'-0".

The member sections used for fabricating the two subassemblages are listed in the insert of Fig. 2. These member sections were designed on the criterion that the beams and columns failed simultaneously by the formation of beam mechanisms and with the assumption that the in-plane behavior of the columns was not impaired by lateral-torsional buckling. In plastic design, it is customarily assumed that the maximum beam moment near the column face exceeds its plastic moment value because of strain-hardening effect. To account for this effect, Ref. 1 recommends that an increase of 10 percent of the plastic moment be included in the design. Accordingly, the criterion for a balanced design for

total collapse of all member components was

$$M_J = 1.10 \, M_p + V \, \frac{d_c}{2} \tag{5}$$

in which M_J = joint moment,

M_p = plastic moment of the beam,

V = shear force at the face of column, and

d_c = depth of column.

It was found after the test of subassemblage S-1 that the maximum moment that could be developed in the beam at the column face was simply M_p, the plastic moment of the beam. Hence in the test of subassemblage S-2, the axial loads on the columns were adjusted so that the criterion for balanced design was then

$$M_J = M_p + V \, \frac{d_c}{2} \tag{6}$$

The principal variable for these tests was the slenderness ratio about the weak axis h/r_y which was 60.0 for subassemblage S-1 and 76.3 for subassemblage S-2. The slenderness ratio about the strong axis was 34.8 and 36.2 respectively. These values were calculated based on the measured dimensions of the column elements of the test specimens.

Details of beam-to-column connections for the two subassemblages are shown in Fig. 3. The two horizontal and the diagonal stiffeners of each joint were of the same thickness as the flanges of the column. The criterion on which the design of stiffeners was based was that no failure should occur in the connection before the subassemblage failed.

A typical load point detail is shown in Fig. 4. All stiffeners were cut from 1/2" plate. They were 1 7/8" wide and their depth varied for each beam as listed in the insert. There were two load points per beam, each located at the quarter span. At each load point, a pin of 1 1/2" diameter x 10" length was welded in the hole in the beam web such that it was perpendicular to the web. Then the vertical and horizontal stiffeners were welded in place.

Each subassemblage was delivered to the laboratory in three pieces: column and two beams. Field welding of the two beams to the column was performed after the column had been set in position in a 5,000,000 lb. universal testing machine.

Details of column end fixtures have been described elsewhere.[7] The roller end supports for the beams and the pin-end link assemblies at the joints that are described in Ref. 7 were used for subassemblage S-2 only. For subassemblage S-1, a special end fixture was fabricated to pin the end of each beam to the supporting tower. However, during the test of S-1, it was found that as the beams began excessively, they pulled the test columns out of alignment. The roller end supports for the beams and the link assemblies were then designed to replace the pin-supports used for subassemblage S-1.

2.2 Testing Arrangement

The testing arrangement is shown diagrammatically in Fig. 5 and a photograph of a test in progress is given in Fig. 6.

The sequence of loading adopted for these tests was as follows:

1. Applied axial load on columns.

2. Loaded both beams incrementally and simultaneously.

3. If no failure occurred, applied more axial load on the columns.

The axial load on the columns was applied through the 5,000,000 lb. universal machine and each beam was loaded by a gravity load simulator through a spreader beam. After each application of load, the test specimen was allowed to stabilize for a few minutes before data were recorded.

In each test, the columns were braced against any adverse out-of-plane movement at every floor level: top of upper column, upper and lower joints and bottom of lower column. The beams were braced at spacing in accordance with the current recommendations.[1,8,9]

2.3 Methods of Data Acquisition

The measurements were strains and deformations. Strain readings were recorded automatically in a B & F 146 channel strain recorder and manually in bridge boxes. The vertical beam deflections were recorded with the aid of a Kern level. Transverse displacements of columns for subassemblage S-1 were measured through three transits each located at the mid-height of every column. For the test of sub-assemblage S-2, lateral column displacements were measured by linearly varying potentiometers. Out-of-plane deformations at midheight of the middle columns were measured with micrometer depth gages. The rotation of every joint was measured by two apparatus; mechanical level bar and electrical rotation gage.

3. CONTROL TESTS

The steel used in the test specimens was purchased as ASTM A36. It was delivered in eight pieces of length varying from about 30 ft. to 46 ft. Table 1 summarizes the steel lengths, the mill yield stress, tensile strength, percent elongation and the chemical composition for the steel. No information was provided by the steel supplier on the 8I18.4 section.

A number of control tests were performed for the purpose of determining the mechanical and geometrical properties of the sections. These tests are summarized in Table 2.

3.1 Tension Tests

At least three tension specimens were cut from each section: one from the quarter point of the top flange, one from the mid-point of the bottom flange and one from the mid-height of the web. These specimens were made in accordance with ASTM Specification No. A370-67 "Mechanical Testing of Steel Products" and tested in accordance with the procedure recommended in Ref. 10. The tests were performed in a 120,000 lb. Tinius-Olsen testing machine. The average yield stresses and other mechanical properties are listed in Table 3.

3.2 Geometrical Properties

The average geometrical properties and the plastic moment capacities of all sections are given in Table 4. These values were computed based on:

(1) the cross section measurements taken by micrometers and calipers at about 3 ft. intervals along the length of each section, and

(2) calculation performed on the contours of the cross-sections drawn on graph sheets. Web thickness could only be measured at every cut made in a length.

3.3 Stub Column Tests

One stub column test was performed on an 8W35 shape and one on an 8W24 shape in accordance with the procedure recommended in the CRC Guide.[3] The results of these two tests are given in Table 5. The non-dimensional load axial vs. deformation curve for 8W35 section is given in Fig. 7, and a photograph of the column of 8W24 section after test is given in Fig. 8. The maximum discrepancy between the experimental value of P_y and the calculated value is about 2 percent. The calculated value in this instance is the average cross-sectional area of the stub column multiplied by the yield stress obtained from tension tests.

3.4 Residual Strain Measurements

Residual strain measurements were made on five specimens: three from 8W35 section and two 8W24 sections. The method of measurement conformed with the procedure recommended in Ref. 11.

A typical measured residual stress pattern is shown in Fig. 9. The broken lines in the same figure is the residual stress pattern customarily assumed in a wide-flange section.[1] Figure 10 shows the average residual stress distributions for the two sections.

3.5 Erection Moments

It was stated in Sect. 2.1 that the subassemblages had welding of the joints done in the laboratory after the column had been placed in the center of the machine. The measured moments for subassemblage S-2 are shown in Fig. 11. No erection moments were taken for subassemblage S-1. For subassemblage S-2, the maximum erection moment in the column (at the lower joint) represented about 8% of the reduced plastic moment M_{pc}.

4. TEST RESULTS

A summary of the test results is given in Table 6. In this table are listed for each subassemblage, the theoretical joint moment capacity M_m, the theoretical moment transmitted from the beam, the measured maximum moment applied at the joint M_j, the M_j/M_m ratio the computed critical moment M_{cr}, the M_j/M_{cr} ratio, and the mode of failure.

The theoretical joint moment capacity was found by compounding the theoretical moment-rotation curves of the columns immediately above and below the joint. The theoretical in-plane $M-\theta$ relationships of each column was developed by using the column-deflection-curve (CDC) method, the details of which are discussed in Refs. 1 and 12. A general computer program in Fortran IV language has been developed to generate the $M-\theta$ curves for the columns.[13] Any residual stress pattern can be used in the computer program. The values of M_m in Table 6 were obtained based on the average residual stress patterns as given in Fig. 10 for the two sections.

The critical moment M_{cr} given in Table 6 for each joint is the smaller of the two values (from two columns) calculated from the CRC interaction formula (see Fig. 1).

4.1 Moment-Rotation Relationships

Measured moment-rotation relationships for the two subassemblages are plotted in Figs. 12 through 15. The methods of computing

the column end moments and the joint moments have been described in an earlier report.[7] The column end moments can only be plotted as long as the columns remained elastic as they were computed from the electrical resistance strain gage readings. In each figure are also plotted the theoretical M-θ curves (broken lines). These curves were developed using the average residual stresses of the sections and the theoretical end moment ratios which were zero for top and bottom columns,-0.980 for the middle column of subassemblage S-1 and -0.848 for the middle column of S-2. Also shown in these two figures are the predicted critical moment M_{cr} for the columns and the joints as computed from Eq. 1. It can be seen that the general shape of experimental and theoretical relationships for the joints are similar.

For the upper joint of S-1, the beam developed mechanism earlier than expected at a load about 7% less than the computed failure load. When applying more axial load on the column in attempting to fail the subassemblage, joint moment dropped with very small increase in rotation. In Figs. 12 and 13, only the experimental results before increasing more axial load are plotted.

4.2 Out-of-Plane Deformations

The lateral displacements of the compression and tension flanges at midheight of the middle column for both subassemblages are shown in Fig. 16. The twisting angle determined from the differential displacement of the flanges are plotted in Fig. 17. At maximum applied moment, the lateral displacements for S-1 were 0.120 in. and 0.029 in. for the compression and tension flanges respectively. For subassemblage S-2, these values were 0.416 in. and 0.179 in. The twisting angle at maximum load was 0.0119 radians for S-1 and 0.0315 radians for S-2.

A comparison shows that at low moment, both columns exhibited very small out-of-plane deformations. However at higher moment, subassemblage S-2 began to deform laterally more than S-1 did. For S-1, unloading did not increase the lateral displacement or twist as much as those for S-2. In S-2, the maximum recorded lateral displacement of the compression flange was 2.57 in. at a joint moment of 338 kip-in. The corresponding twist was 0.178 radians.

4.3 Twisting Moments

Twisting moments at nine sections of the columns of every subassemblage were computed from the recorded strain gage readings. The procedure for analyzing the recorded·strains has been described in an earlier report.[7] Figure 18 shows the location of these nine sections along the length of the columns. The twisting moment vs. joint rotation relationship for every column of the two subassemblages are plotted in Figs. 19 through 24. Only the values that were computed from strain readings taken before yielding occurred are shown. The curves are rather scattered and there is no definite pattern from which a conclusion can be drawn. Nevertheless, these results are presented for possible use in future studies. Within the elastic range, the twisting moments were, on the whole, rather small in comparison with the reduced plastic moment M_{pc} of each column.

4.4 Behavior at Loads Approaching Failure and Modes of Failure

a) Subassemblage S-1

In subassemblage S-1, yielding was first observed at a column load of 140 kips on the west flange of the middle column at the lower joint level. When the full amount of the calculated axial

load of 173 kips (P/P_y = 0.50) was applied on the column before application of beam loads, yield lines appeared in the east column flange at the upper joint level. These yield lines were probably caused by the concentration of high residual stresses due to welding of stiffeners to form the joint. On applying the first beam load, tensile yield lines appeared in the top flange of the upper beam adjacent to the upper joint. At a total load of 26 kips on the upper beam, the midheight of the compression flange of the middle column yielded. This yielding spread immediately over the full length of the column on the next increment of beam load of 2 kips.

Noticeable twisting occurred when the lower joint moment was about 708 kip-in. (see Fig. 17). The upper beam failed by the formation of beam mechanism at a load less than the predicted load. When this situation occurred, the hydraulic supply to the tension jack for the upper beam was then blocked and more oil was pumped into the jack for the lower beam in order to fail the lower joint. The moment-carrying capacity of the lower joint was finally exhausted at a total load of 42.0 kips. At this stage, however, there was no sign of unloading even though a plastic hinge had developed at the top of the lower column. It was noticed that as the load on the lower beam was increased, that on the upper beam began to drop gradually. When the lower beam failed, the upper beam load had dropped from a total of 37.4 kips to 32.2 kips.

Figure 25 shows the in-plane deflection profile of the sub-assemblage at three selected load levels. At the first load level, the subassemblage remained essentially elastic and there was no lateral

or torsional deformation in any of the members. The second load level

is the level at which significant yielding was observed in the upper

beam. The third load level corresponds to the load that caused failure

of the lower beam. The recorded deflections indicate that, as the

applied loads approached their maximum values, the beams continued to

deflect at an increasing rate, while the column deflections increased

only slightly.

After both beams had failed, more axial load was then applied

to the columns. The additional axial load resulted in further release

of the joint moments. The subassemblage finally failed at a column

load of 244 kips--some 71 kips higher than the initially applied load.

This increase was equivalent to a P/P_y ratio of 0.206. The vertical

load on the upper beam was 30.0 kips and that on the lower beam was

28.6 kips when unloading occurred in the columns. Figure 26 shows

the shape of the subassemblage after testing.

As given in Table 6, the initial failure mode was the formation

of beam mechanism, followed by failure of the lower joint and excessive

twisting in every column and beam. In Fig. 27 are shown the locations

of plastic hinges and failure modes of the members in the subassemblages.

Briefly there were two hinges in the upper beam, one in the lower

beam and the fourth at the top of the lower column. Excessive

twisting occurred at the midheight of every column, and in the spans

between the load points of the beams. In addition to excessive twisting,

the lower column also exhibited local buckling at about its midheight.

Figure 28 shows yield lines penetrating across the depth of the section

immediately below the lower joint. Significant lateral-torsional deforma-

tions were observed in the beams between the lateral supports (Fig. 29).

b) Subassemblage S-2

An axial force of 137 kips (corresponding to a P/P_y ratio of 0.55) was gradually applied to the columns and was maintained throughout the test. Yielding was first observed in the column flange at the lower joint at a beam load of 4 kips. Yield lines next appeared in the column flange at the upper joint. When both beams were loaded to 11 kips each, tensile yield lines were seen in the top flange of the lower beam. At the same time, the compression flange of the middle column began to yield. This yielding penetrated rapidly into the web as the beams were loaded further. Although the columns began to deflect noticeably out of its plane at a lower joint moment of about 400 kip-in., they were still able to sustain higher moments transmitted from the beams. At a beam load of 25.8 kips, the capacities of the three columns were reached but the column load did not drop. Next, more oil was pumped into the hydraulic jacks of the simulators for the two beams in order to deform the beams further while maintaining the column load of 137 kips. The joints were found to be able to sustain larger rotations before the columns unloaded, at which time the rotation of the lower joint was about four times its rotation at the maximum load. For the upper joint the maximum rotation just before the columns unloaded was about twice the maximum load rotation.

The deflected configurations of the subassemblage at four selected load levels are shown in Fig. 30. The entire subassemblage was in the elastic range at the first load level. No significant lateral deflection or twist was observed in the three columns. At the second load level, the beam loads were sufficiently large to cause the columns to deflect laterally and twist (see Fig. 17). The

in-plane deformations of the beams and columns also increased appreciably.
The third load level corresponds to the situation that maximum resisting
moment has just attained at the upper and lower joints. Beyond this
load, the resisting moment of the joints started to decrease, causing
a reduction of the beam loads. This was observed at the fourth load
level. Unlike the columns in subassemblage S-1 (see Fig. 25), the columns
in this subassemblage deflected significantly in the plane of bending.

Close-up views of the middle and lower columns after testing
are shown in Figs. 31 and 32. The yield patterns in these figures
suggest that severe twisting occurred at the center of the middle
column and in the upper half of the lower column.

5. DISCUSSION OF TEST RESULTS

5.1 Influence of Residual Stresses on In-plane M-θ Relationships

The selection of the member shapes in the preliminary design was based on handbook values [14] and the in-plane moment-rotation curves were interpreted from the charts in the design aids of Ref. 1. As is common in most laboratory tests, the geometrical and mechanical properties of the ordered steel were found different from the handbook values. Thus, a completely new analysis was performed for the in-plane M-θ curves in order that the experimental results could be compared in a valid manner. As mentioned earlier, the theoretical in-plane M-θ curves, as shown in Figs. 12 through 15, were developed not only based on the true geometrical and mechanical properties of the steel, but also on the average measured residual stresses as shown in Fig. 10. If the customarily assumed residual stress pattern (dotted lines in Fig. 10) is used in the analysis, the resulting M-θ curves would be different. Shown in Figs. 33 and 34 are the in-plane M-θ curves based on the measured residual stresses, those based on the assumed residual stresses, and the experimental curves for subassemblages S-1 and S-2. In all cases, the M-θ curves based on the assumed residual stresses exhibit relatively stiffer slope than those based on the measured residual stresses. With the exception of the lower joint of S-2, all predicted in-plane maximum moment capacities based on assumed residual stresses are somewhat higher. For the lower joint of S-2, the predicted maximum capacity is identical for the two separate analyses.

5.2   Loss of In-plane Capacity due to Lateral-Torsional Buckling

The experimental results correlate remarkably well with the in-plane M-θ curves based on measured residual stresses even though the columns exhibited out-of-plane deformations before the maximum capacities were reached.   (See Figs. 16 and 17).   In subassemblage S-1, if the upper beam were not exhausted before the predicted load, the maximum moment capacity of the upper joint could be reached, as evident from the experimental curve whose slope was still relatively stiff before unloading.   The reason for the upper beam to fail before the predicted load is that tensile force had developed in this beam. This was the direct consequence of the pins being used to support the beams of subassemblage S-1.   The ratios of experimental maximum moment to theoretical maximum moment have been given in Table 6.   There was no loss in the moment-carrying capacity for the lower joint of S-1 or S-2.   For the upper joint of S-2, the loss in in-plane capacity due to lateral-torsional buckling was only about 6 percent.

5.3   Post-Buckling Strength and Behavior

Subassemblage S-1 was primarily designed to fail by lateral-torsional buckling of the middle column at a load of about 95 percent of the predicted in-plane capacity of both joints.   The analysis based on the measured residual stresses, which was performed after the test, showed, however, that the predicted lateral-torsional buckling moment had been shifted to almost coincide with the in-plane maximum capacity for the lower joint.   The test results seem to indicate that maximum in-plane capacity did reach but because the columns did not fail, it was impossible to evaluate their true behavior on the unloading path.

Subassemblage S-2 was initially designed on the criterion
that all three columns would fail by lateral-torsional buckling before
their respective in-plane capacity was reached. The new analysis
based on the measured residual stress pattern did not change the
original intention. In fact, the critical moment M_{cr} was almost
identical for the two analyses. The results presented in Figs. 14,
15 and 34 demonstrate that not only were the critical moments M_{cr}
for the two joints surpassed, but the strength and behavior of the
lower joint almost coincide with the theoretical prediction for
in-plane behavior. In fact, the experiment curve exhibits greater
rotation on the unloading path presumably due to strain-hardening
effect. The rotation capacity for the upper joint after the attainment
of maximum moment was slightly less than prediction. Table 6 shows
that the loss in in-plane capacity for the upper joint due to lateral-
torsional buckling was very small. There was no loss in the in-plane
capacity for the lower joint. In relation to the critical moment,
there was an increase of about 34 percent moment capacity for the
upper joint, and about 51 percent for the lower joint. These results
demonstrate a substantial post-buckling strength that is currently
neglected in the design of laterally unsupported columns.

5.4 Prediction of Lateral-Torsional Buckling by the CRC Formula (Eq. 1)

Lateral-torsional buckling is an instability phenomenon which
can physically occur only in a perfectly straight column. However,
in reality, no columns are straight. Thus they are usually in a state
of biaxial stress resulting in in-plane and out-of-plane defor-
mations even in early stages of loading. This point is supported by
the measured out-of-plane deformations as shown in Figs. 16 and 17.

The predicted critical moments tabulated in Table 6 have been calculated on the assumption that the columns were straight. The value of theoretical critical moment for the lower joint of S-1 was 740 kip-in. while that for the lower joint of S-2 was 353 kip-in. The experimental curves in Figs. 16 and 17 have no bifurcation points. However if bifurcation point is assumed to be one from which excessive deviation from the linear portion of the experimental moment-twist curve begins, then the experimental critical moments are about 710 kip-in. for S-1 and 380 kip-in. for S-2 (see Fig. 17). These values are in reasonably good agreement with the theoretical critical moments. Research is currently underway on theoretical prediction of the initiation of lateral-torsional buckling of continuous beam-columns,[15] the results of which may be used to compare with the experimental values reported herein and the simplified CRC formula (Eq. 1).

6. CONCLUSIONS

Based on the results presented in this paper, the following conclusions may be drawn:

1. There is a substantial post-buckling strength for laterally unsupported columns ($h/r_y \leq 76$) in a continuous frame. This post-buckling strength is found to be as high as 51 percent of the buckling strength as computed from the CRC Interaction formula (Eq. 1)

2. The in-plane behavior for laterally unsupported columns ($h/r_y \leq 76$) in a continuous frame follows closely for laterally unsupported column. The reduction in rotation capacity due to lateral-torsional buckling is almost negligible.

3. The effect of strain-hardening in the beam was found to be insignificant and may be ignored in the design of columns.

4. The current design procedure for laterally unsupported columns is conservative.

5. The unloading occurred on the beam as more axial load was applied on the columns of S-1 indicates that failure is likely to occur in the beam under gradually increasing axial load.

6. A comparative study on the influence of residual stresses shows that in-plane moment-rotation relationship is sensitive to different residual stress patterns.

7. <u>ACKNOWLEDGMENTS</u>

8. <u>NOTATION</u>

The following symbols are used in this paper:

A	=	area;
b	=	flange width;
C_m	=	end-moment correction factor;
d	=	depth of section;
d_c	=	depth of column;
d_s	=	depth of stiffener;
E	=	elastic modulus;
E_{st}	=	strain-hardening modulus;
h	=	height of column in test specimen;
I	=	moment of inertia, subscripts x and y denote axes;
M_{cr}	=	critical moment;
M_J	=	maximum applied joint moment;
M_m	=	maximum joint moment capacity based on in-plane behavior;
M_o	=	maximum moment which the columns can sustain if no axial load is present;
M_p	=	plastic moment of beam;
M_{pc}	=	reduced plastic moment;
P	=	axial load on column;
P_e	=	elastic buckling load about x axis;
P_o	=	maximum load which the column can sustain if no bending moment is present;
P_y	=	yield load of column;
q	=	end-moment ratio;

r = radius of gyration, subscripts x and y denote axes;

t = flange thickness;

V = shear force in beam at face of column;

σ_y = static yield stress of material; and

σ_u = tensile strength of material.

TABLE 1 - MATERIAL SUMMARY

Section (1)	Length (2)	Use (3)	Mill yield stress in kips per square inch (4)	Mill Tensile stress in kips per square inch (5)	Elongations (8 in) as a percentage (6)	Mill Chemical Analysis			
						C (7)	Mn (8)	P (9)	S (10)
8W35	40'-0" 29'-11½"	Column (S-1)	46.50	66.99	25.7	0.22	0.55	0.006	0.026
10W21	46'-0"	Upper Beam (S-1)	46.89	67.52	25.5	0.21	0.63	0.010	0.029
12B16.5	40'-0"	Lower Beam (S-1)	47.53	68.35	25.8	0.15	0.62	0.010	0.026
8W24	40'-0" 28'-3/4"	Column (S-2)	43.57	71.65	28.0	0.20	0.59	0.009	0.022
8I18.4	46'-0"	Upper Beam (S-2)	NOT REPORTED						
8B15	40'-0"	Lower Beam (S-2)	43.75	62.16	26.4	0.14	0.63	0.011	0.035

TABLE 2 - SUMMARY OF CONTROL TESTS

Subassemblage (1)	Section (2)	Tension Tests (3)	Stub Columns (4)	Residual Strain Measurements (5)	Cross- Section Measurements (6)
S-1	8W35	3	1	3	145
	10W21	6	-	-	42
	12B16.5	4	-·	-	61
S-2	8W24	3	1	2	155
	8I18.4	3	-	-	31
	8B15	5	-	-	80

TABLE 3 - AVERAGE MECHANICAL PROPERTIES

Subassemblage (1)	Section (2)	Specimen cut from (3)	No. of specimens (4)	Static yield stress, σ_y, in kips per square inch (5)	Strain at onset of strain hardening, ϵ_{st} (6)	Strain hardening modulus, E_{st2} in kips per square inch (7)	Tensile strength, σ_u, in kips per square inch (8)	Elongation (8 in) as a percentage (9)
S-1	8W35	flange	2	32.7	0.0160	550	59.9	30.2
		web	1	32.9	0.0200	496	58.7	32.5
	10W21	flange	4	36.2	0.0219	470	60.9	31.2
		web	2	41.0	0.0255	512	63.7	30.4
	12B16.5	flange	3	36.4	0.0251	385	58.0	30.0
		web	1	40.1	0.0240	412	60.3	26.6
S-2	8W24	flange	2	34.4	0.0206	463	61.0	30.6
		web	1	34.8	0.0200	451	60.7	30.3
	8I18.4	flange	2	34.2	0.0189	469	53.6	29.0
		web	1	41.7	0.0218	371	62.5	30.0
	8B15	flange	4	34.6	0.0230	370	57.5	30.4
		web	1	40.3	0.0235	372	60.3	29.1

TABLE 4 - AVERAGE GEOMETRICAL PROPERTIES

Subassemblage	Section	Flange width, b, in inches	Depth, d, in inches	Area, A, in square inches	Moment of inertia about x-x axis, I_x, in inches^4	Moment of inertia about y-y axis, I_y, in inches^4	Radius of gyration about x-x axis, r_x, in inches	Radius of gyration about y-y axis, r_y, in inches	Plastic moment, M_p, in kip inches
(1)	(2)	(3)	(4)	(5)	(6)	(7)	(8)	(9)	(10)
	8W35	8.03	8.16	10.04	124.8	41.9	3.52	2.04	1173
S-1	10W21	5.75	9.78	5.96	100.0	10.42	4.09	1.32	849
	12B16.5	4.04	12.11	5.32	115.6	3.25	4.67	0.78	851
	8W24	6.51	7.93	7.21	82.45	18.58	3.38	1.61	802
S-2	8I18.4	4.09	8.05	5.47	59.7	3.95	3.30	0.85	601
	8B15	4.10	8.18	4.54	49.9	3.74	3.32	0.91	504

TABLE 5 - STUB COLUMN TESTS

Section	Specimen length, L, in inches	L/r_y	b/t	Area, A, in square inches	Calculated axial yield load, $P_{y(cal)}$, in kips	Experimental axial yield load, $P_{y(exp)}$, in kips	$\dfrac{P_{y(exp)}}{P_{y(cal)}}$
(1)	(2)	(3)	(4)	(5)	(6)	(7)	(8)
8W35	27	13.2	16.6	10.39	340	346	1.018
8W24	27	16.8	16.2	7.20	249	251	1.008

TABLE 6 - SUMMARY OF TEST RESULTS

Subassemblage (1)	S-1		S-2	
	Upper Joint (2)	Lower Joint (3)	Upper Joint (4)	Lower Joint (5)
Theoretical joint capacity, M_m in kip-inches	921	742	695	532
Theoretical maximum moment from beam, $M_p + V \dfrac{d_c}{2}$, in kip-inches	935	953	664	564
Measured maximum applied moment, M_j in kip-inches	865	747	652	532
M_j/M_m	0.939	1.007	0.938	1.000
Computed critical moment for joint, M_{cr}, in kip-inches	--	740	485	353
M_j/M_{cr}	--	1.009	1.344	1.507
Mode of Failure	Mechanism developed in the upper beam, followed by failure of lower joint.		Twisting in middle and lower columns	
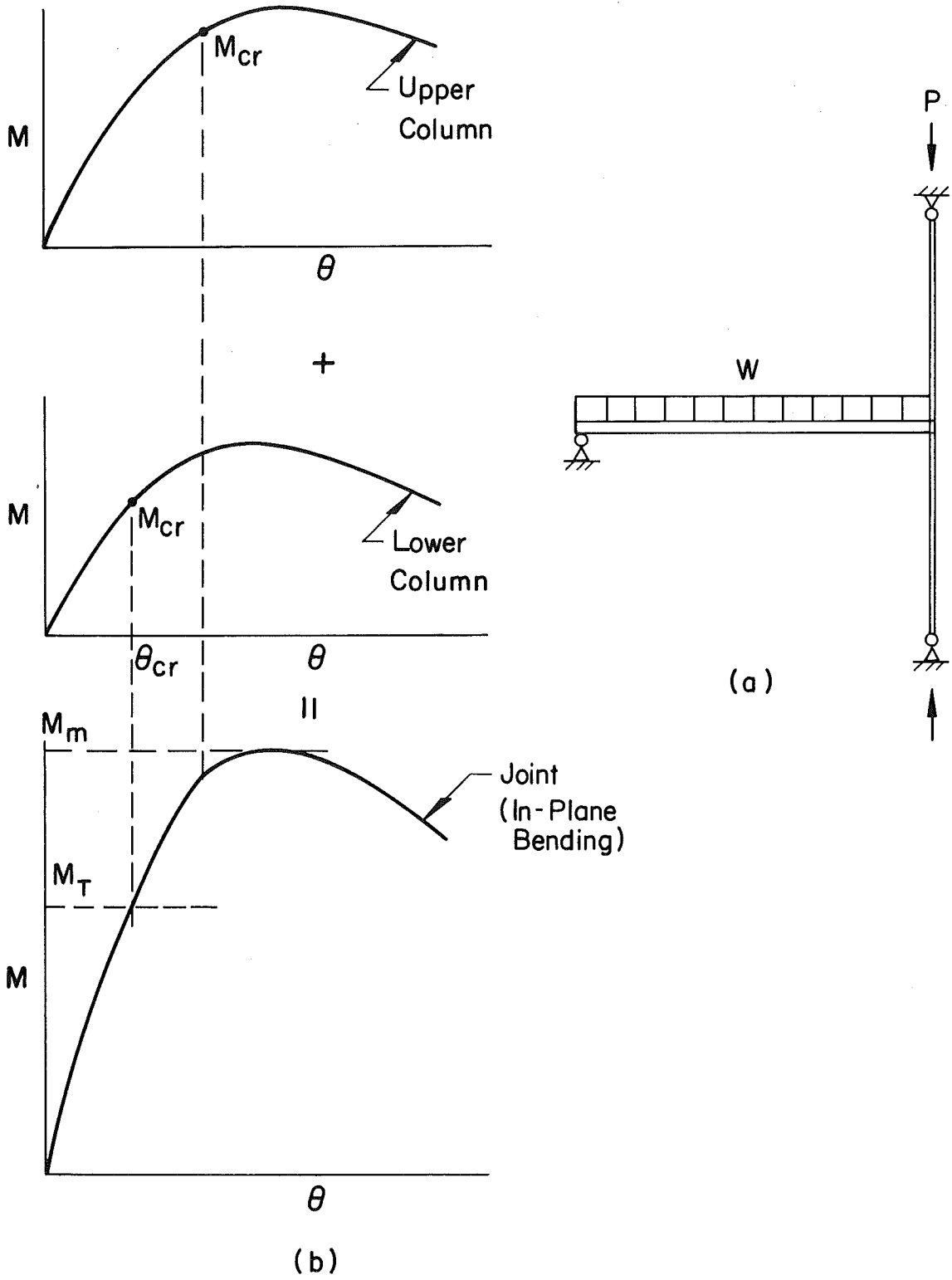
Fig. 1 Resisting Moment of a Subassemblage
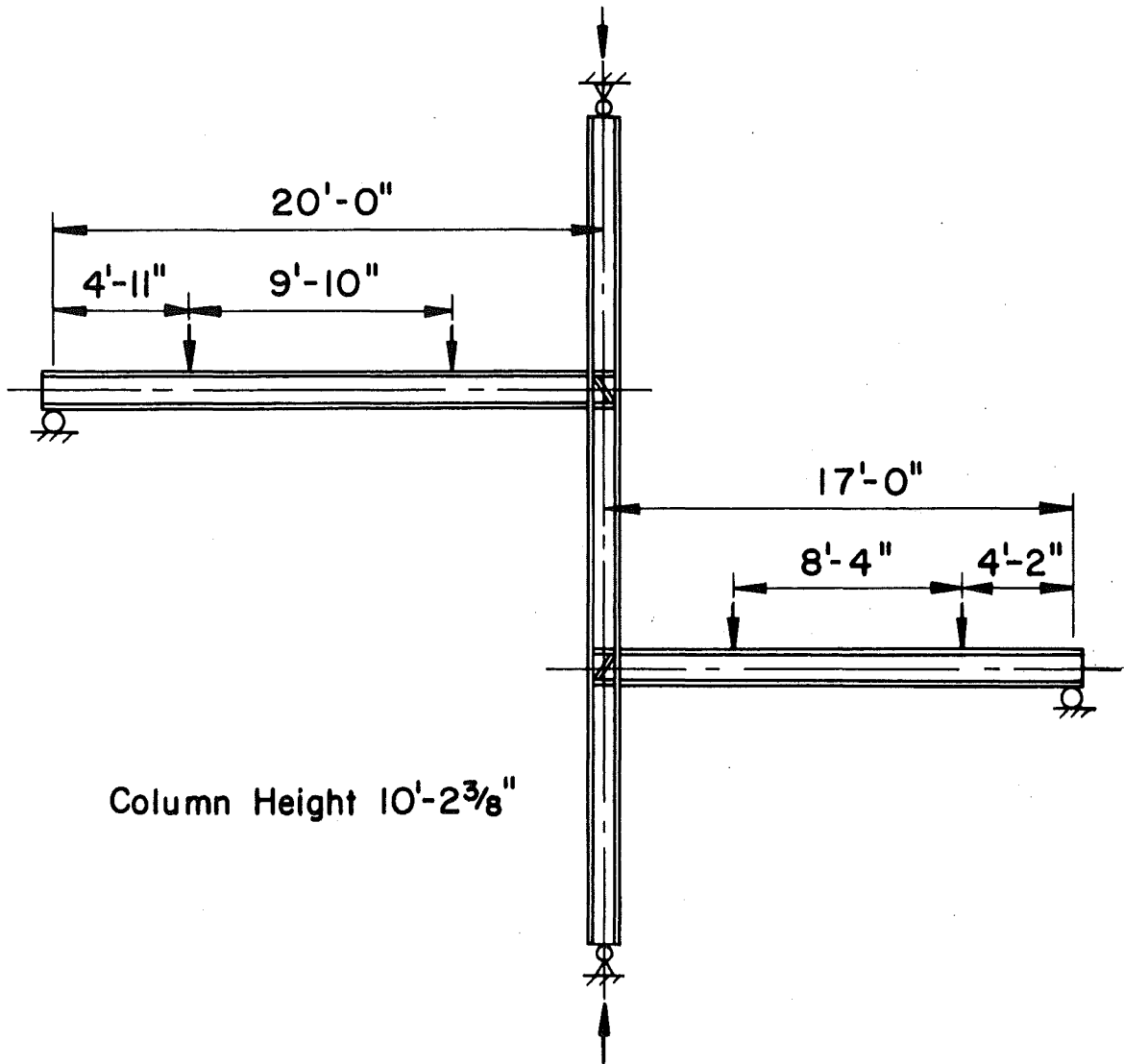
Column Height 10'-2⅜"

SUBASSEMBLAGE	COLUMN	$\dfrac{h}{r_x}$	$\dfrac{h}{r_y}$	UPPER BEAM	LOWER BEAM
S-1	8W35	34.8	60.0	10W21	12B16.5
S-2	8W24	36.2	76.3	8I18.4	8B15

Fig. 2 Test Specimens
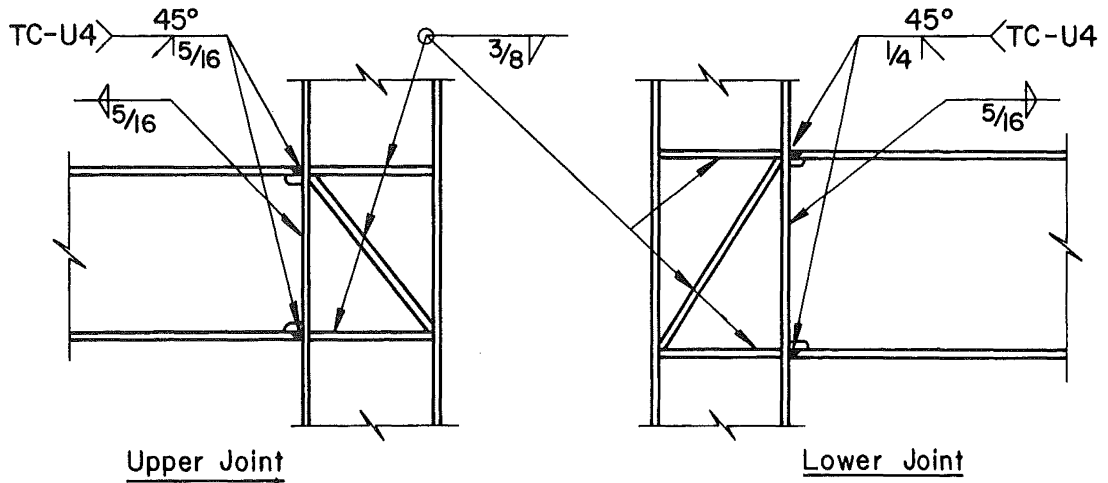
(a) Subassemblage S-1
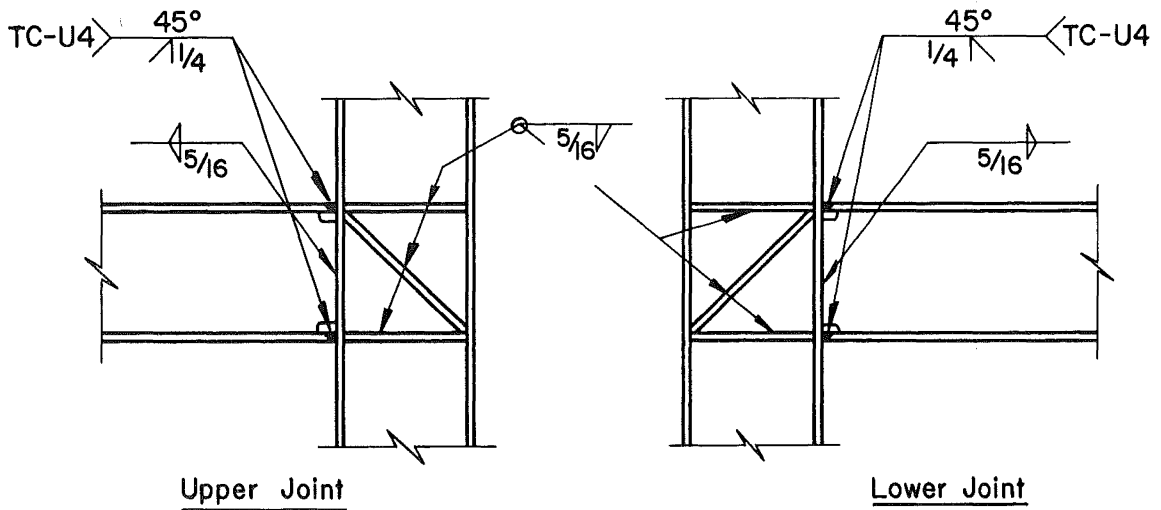
(b) Subassemblage S-2

Fig. 3   Joint Connection Details
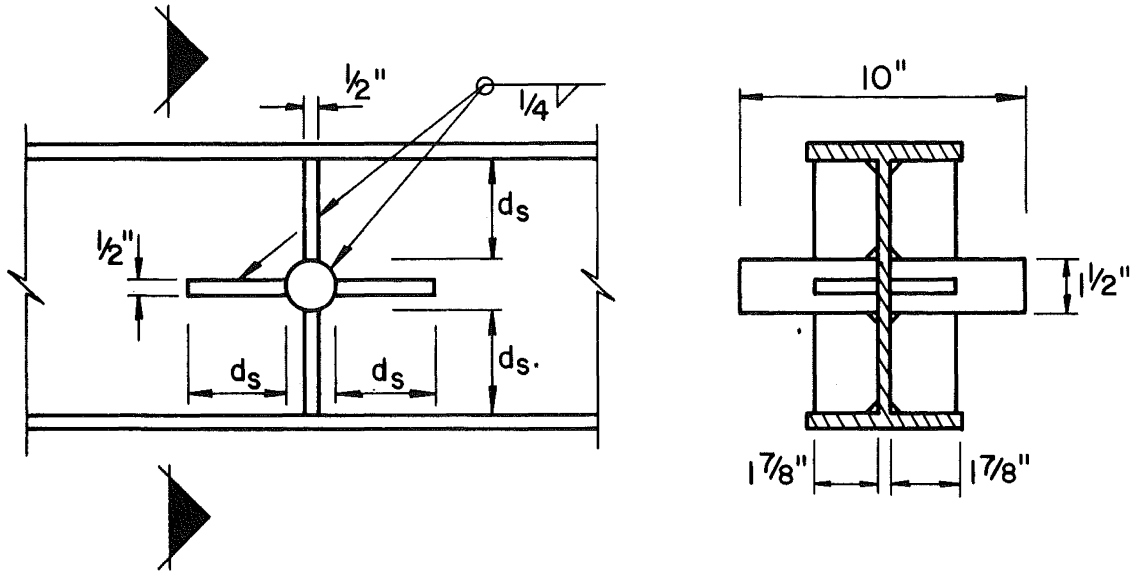
Subassemblage	Beam	d (in.)
S - 1	10 WF 21	3 7/8
	12 B 16.5	5
S - 2	8 I 18.4	2 13/16
	8 B 15	3

Fig. 4   Load Point Details
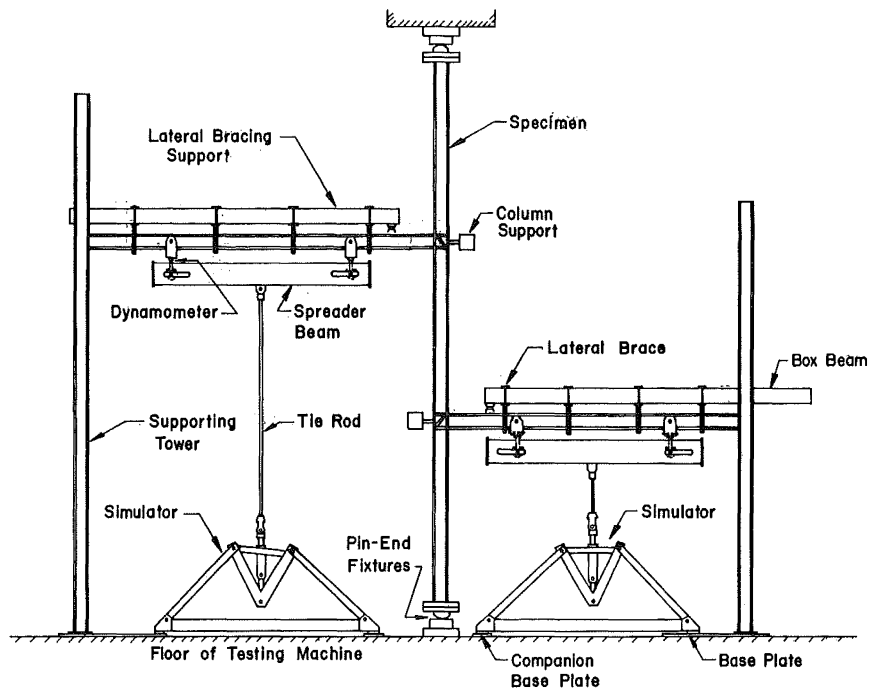
Fig. 5   Test Setup
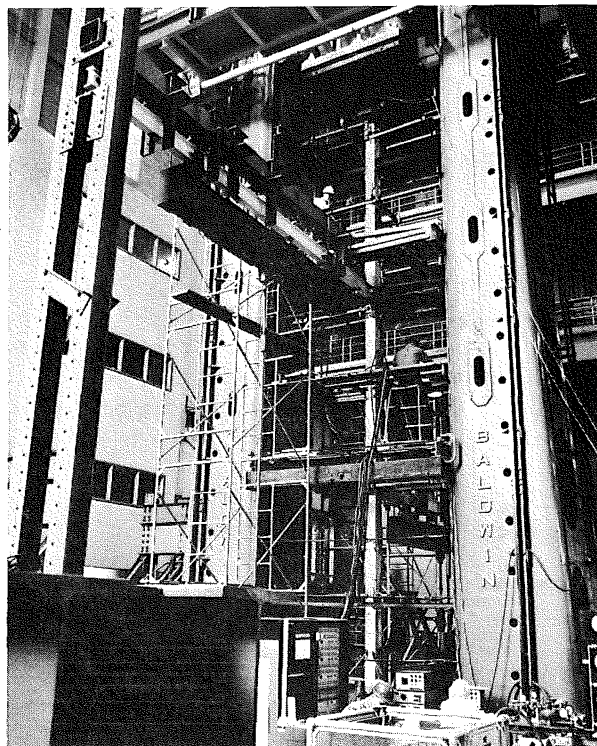
Fig. 6   Test in Progress
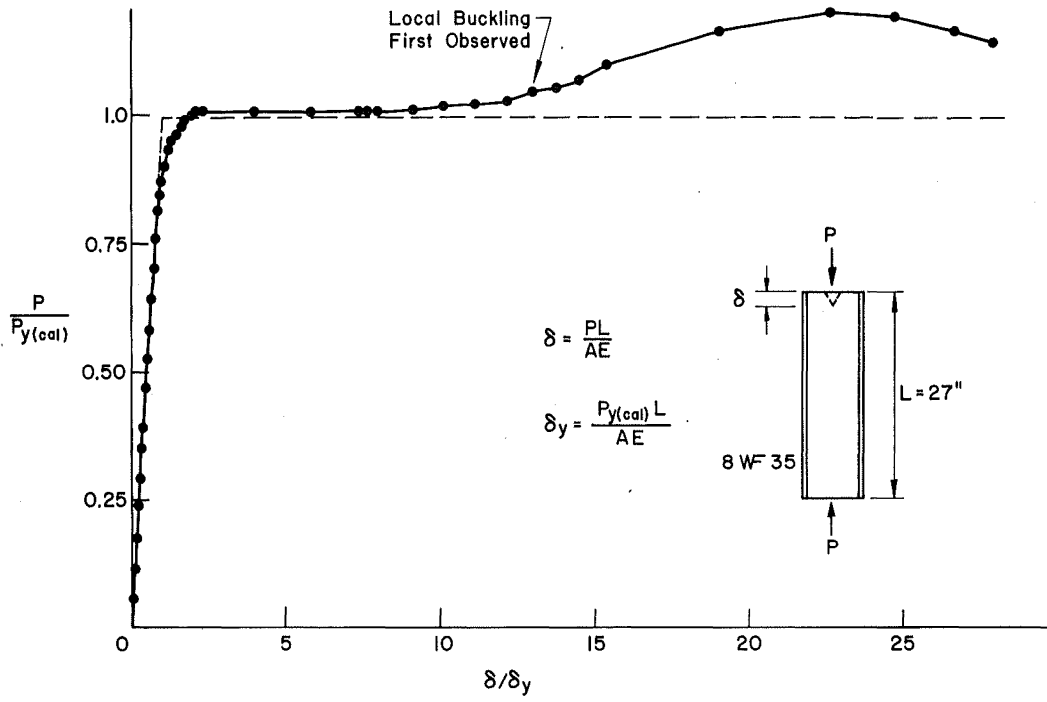
Fig. 7   Stub-Column Test Results
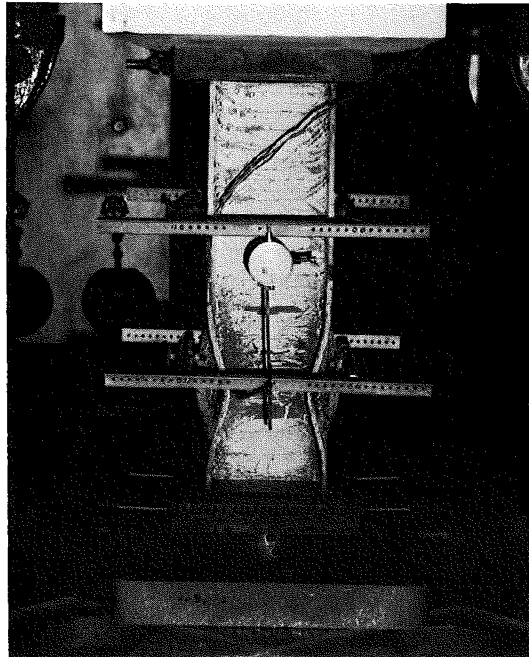
Fig. 8   8W24 Stub-Column After Test
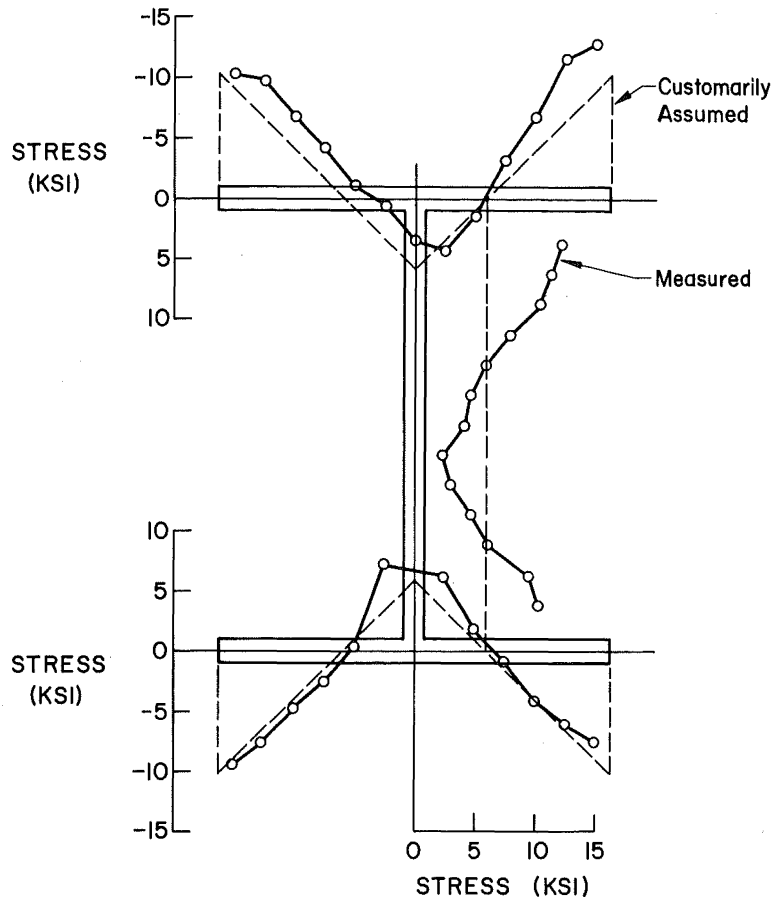
Fig. 9   Sample Residual Stress Pattern (8W24)
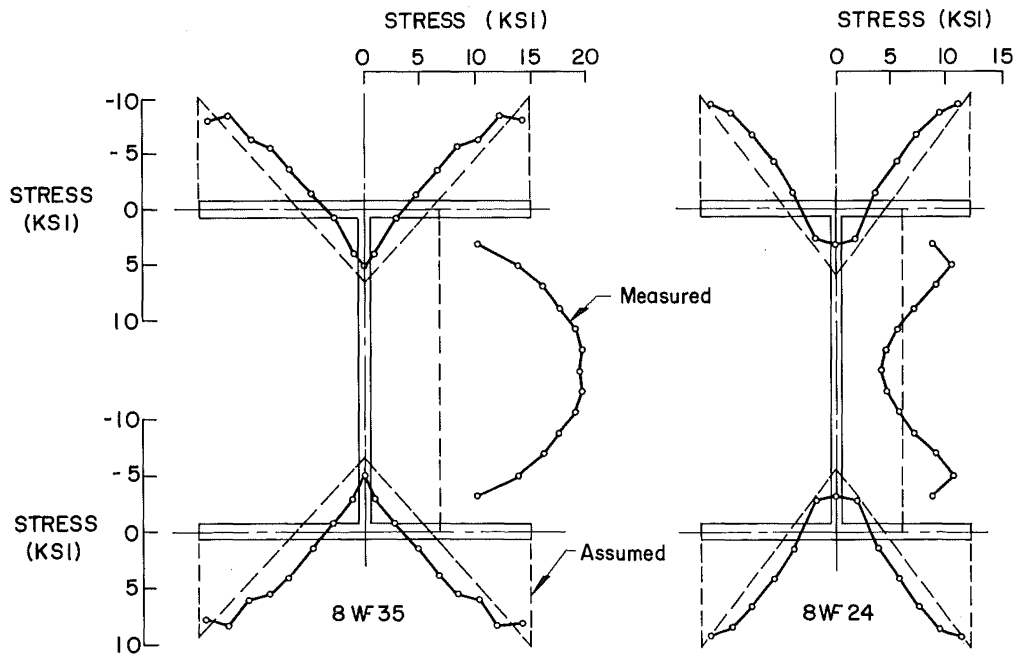
Fig. 10   Average Residual Stress Patterns of 8W35 and 8W24 Sections

Beam ($\xrightarrow{\ +\ }$)

Positive
Moment

Column

Moment Scale

0   20   40   60
KIP - IN.
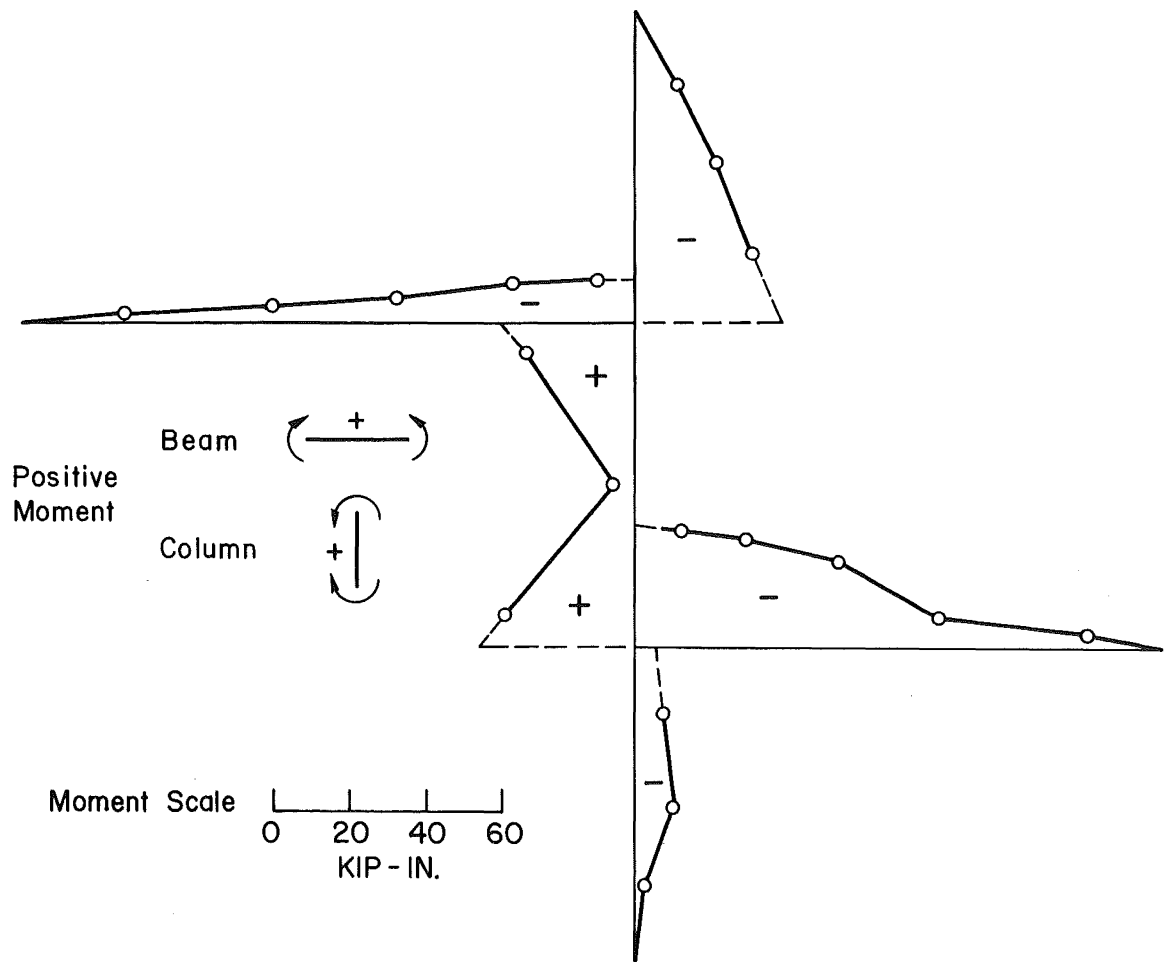
Fig. 11   Erection Moments for Subassemblages S-2
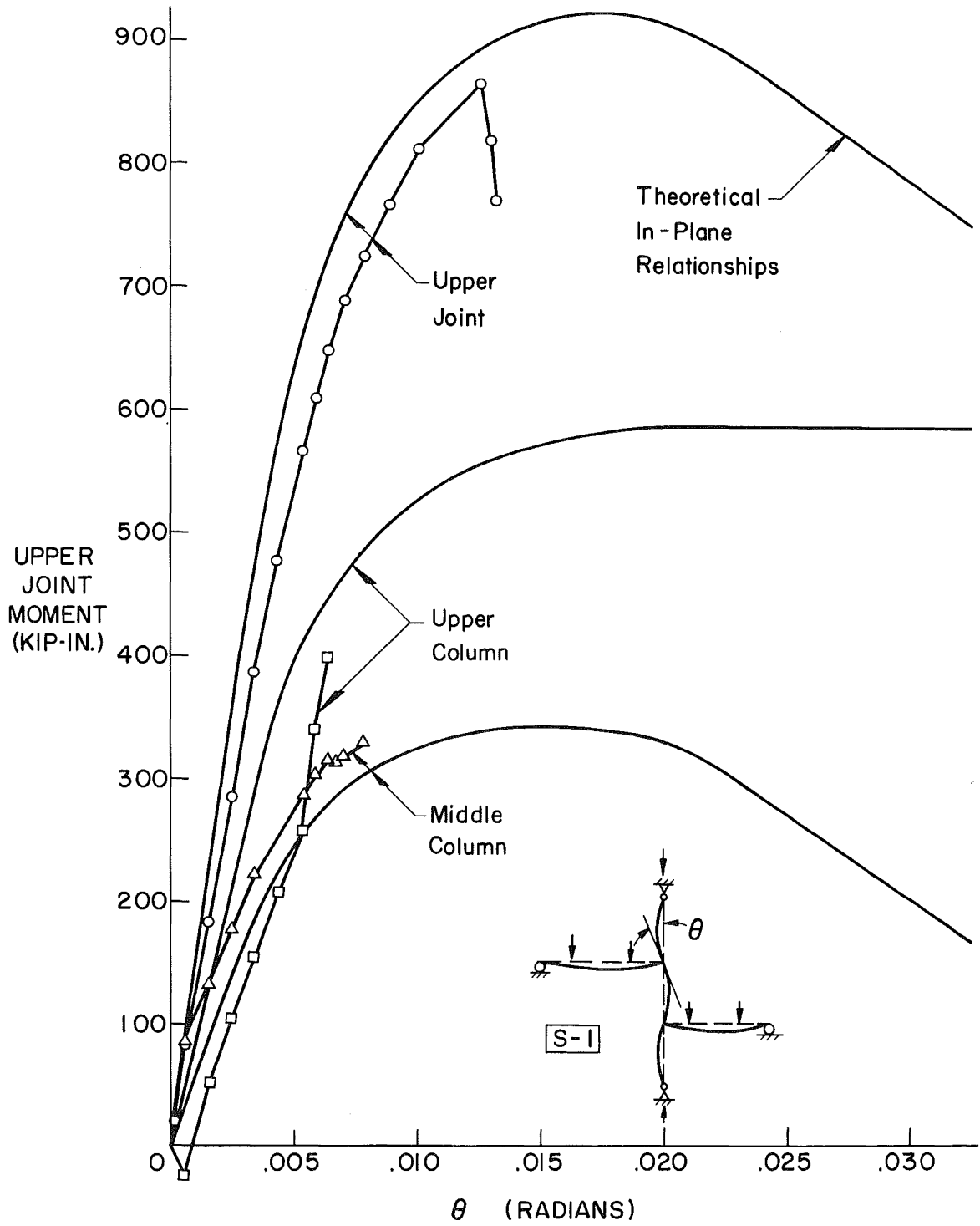
Fig. 12   Moment-Rotation Relationships for Upper Joint of Subassemblage S-1
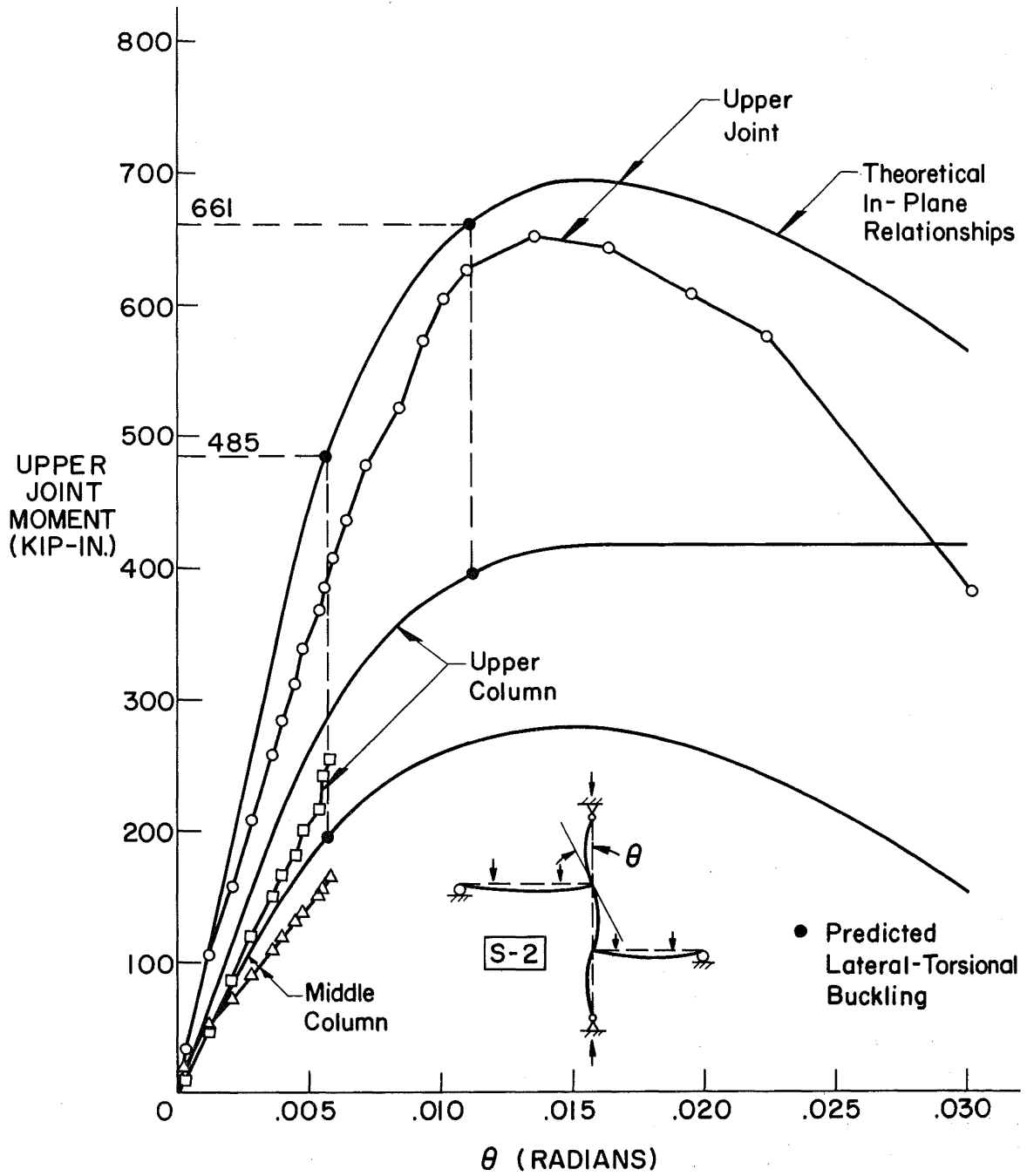
Fig. 13 Moment-Rotation Relationships for Lower Joint of Subassemblage S-1
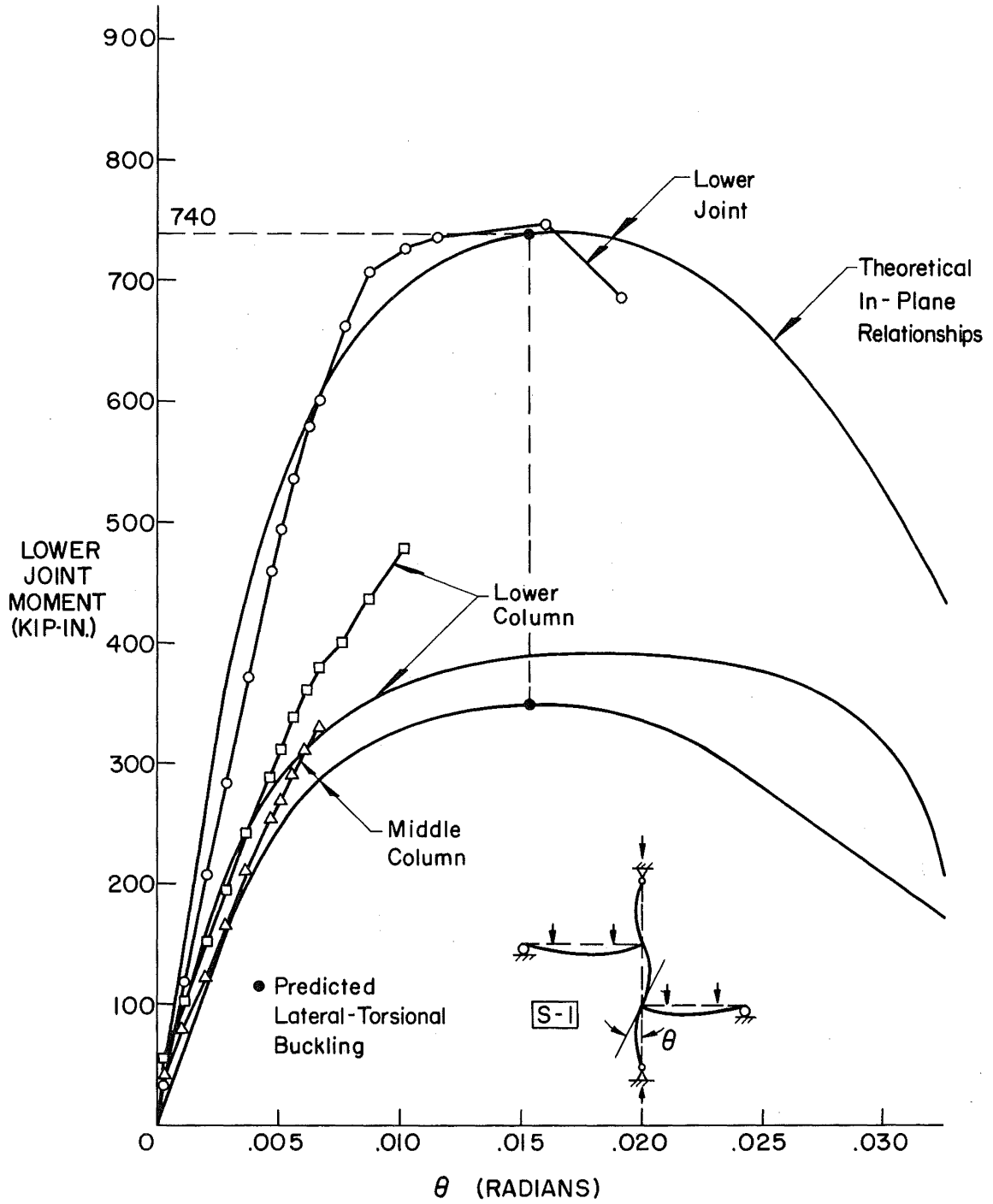
Fig. 14   Moment-Rotation Relationships for Upper Joint of Subassemblage S-2
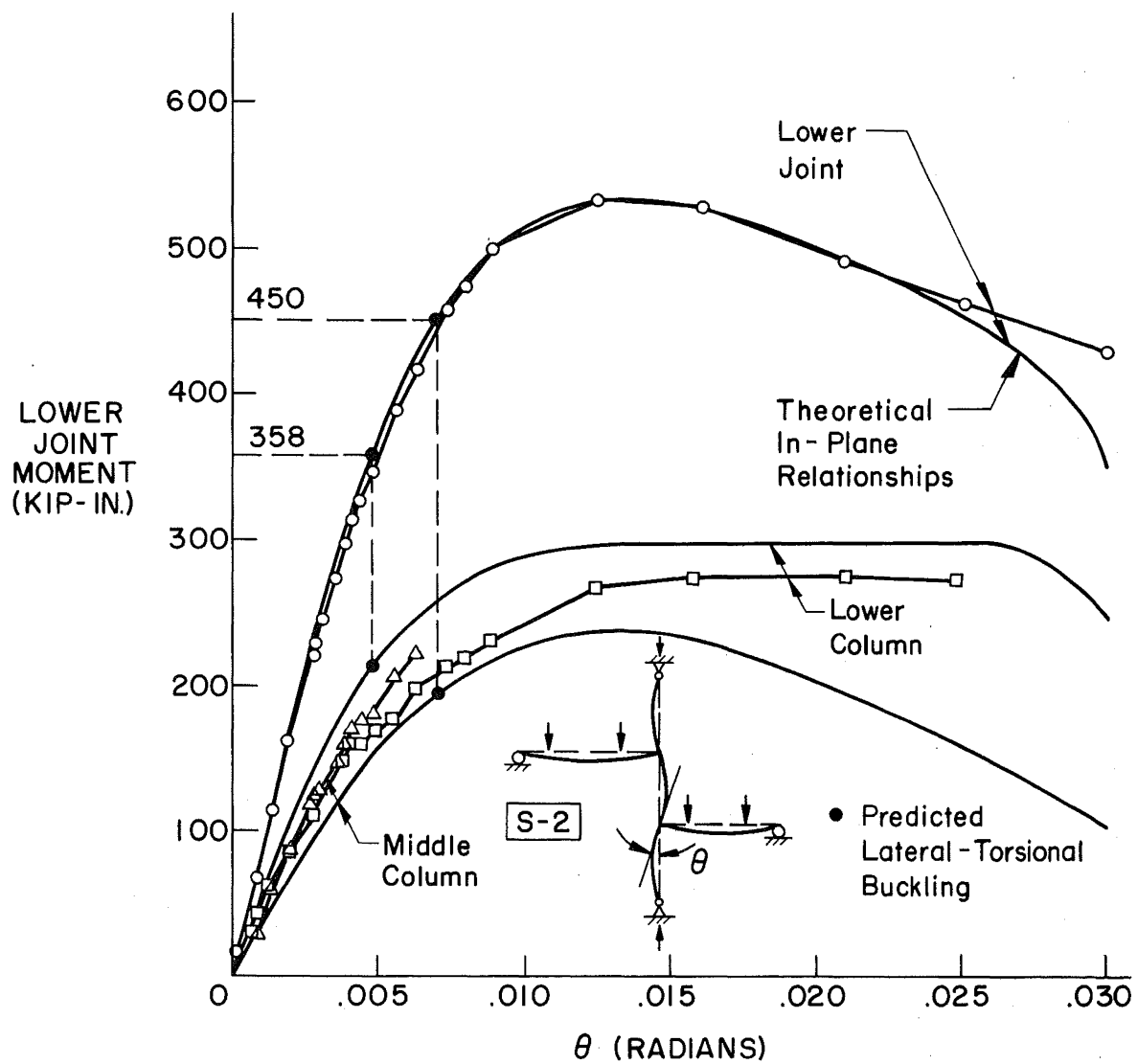
Fig. 15 Moment-Rotation Relationships for Lower Joint of Subassemglage S-2
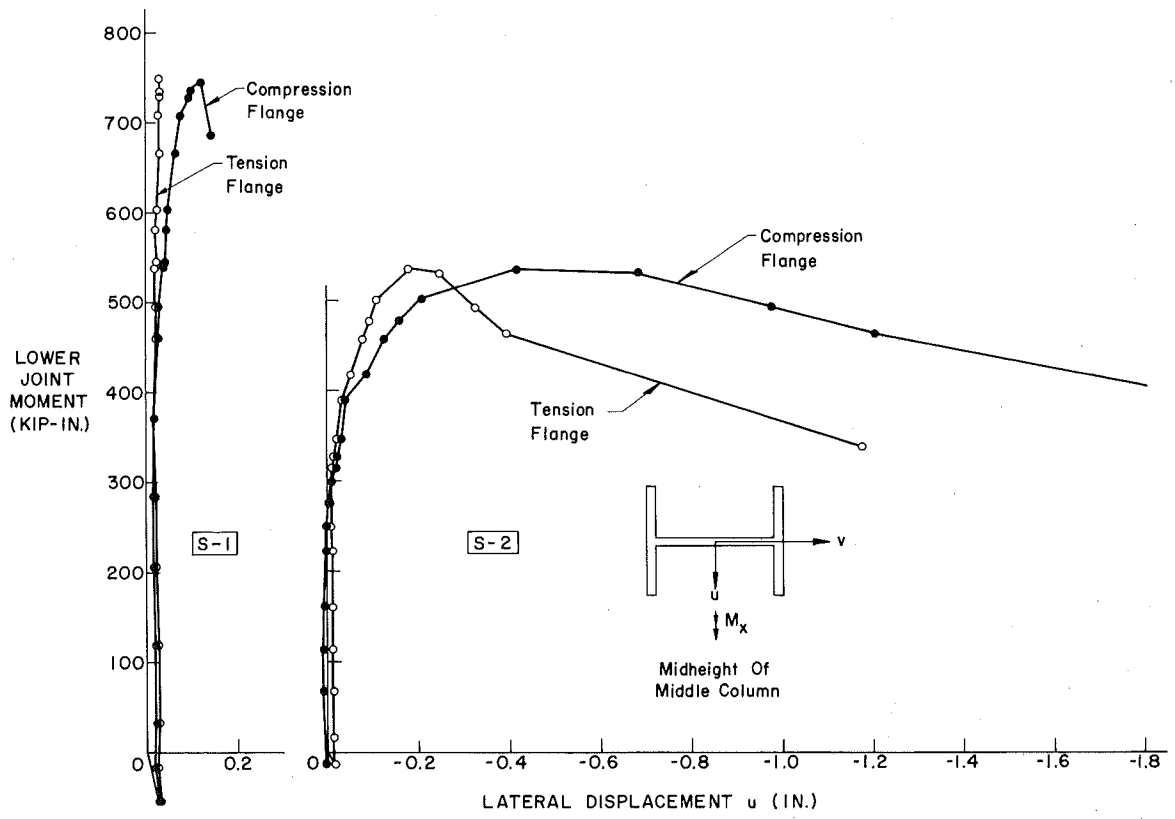
Fig. 16 Lateral Displacement of Columns
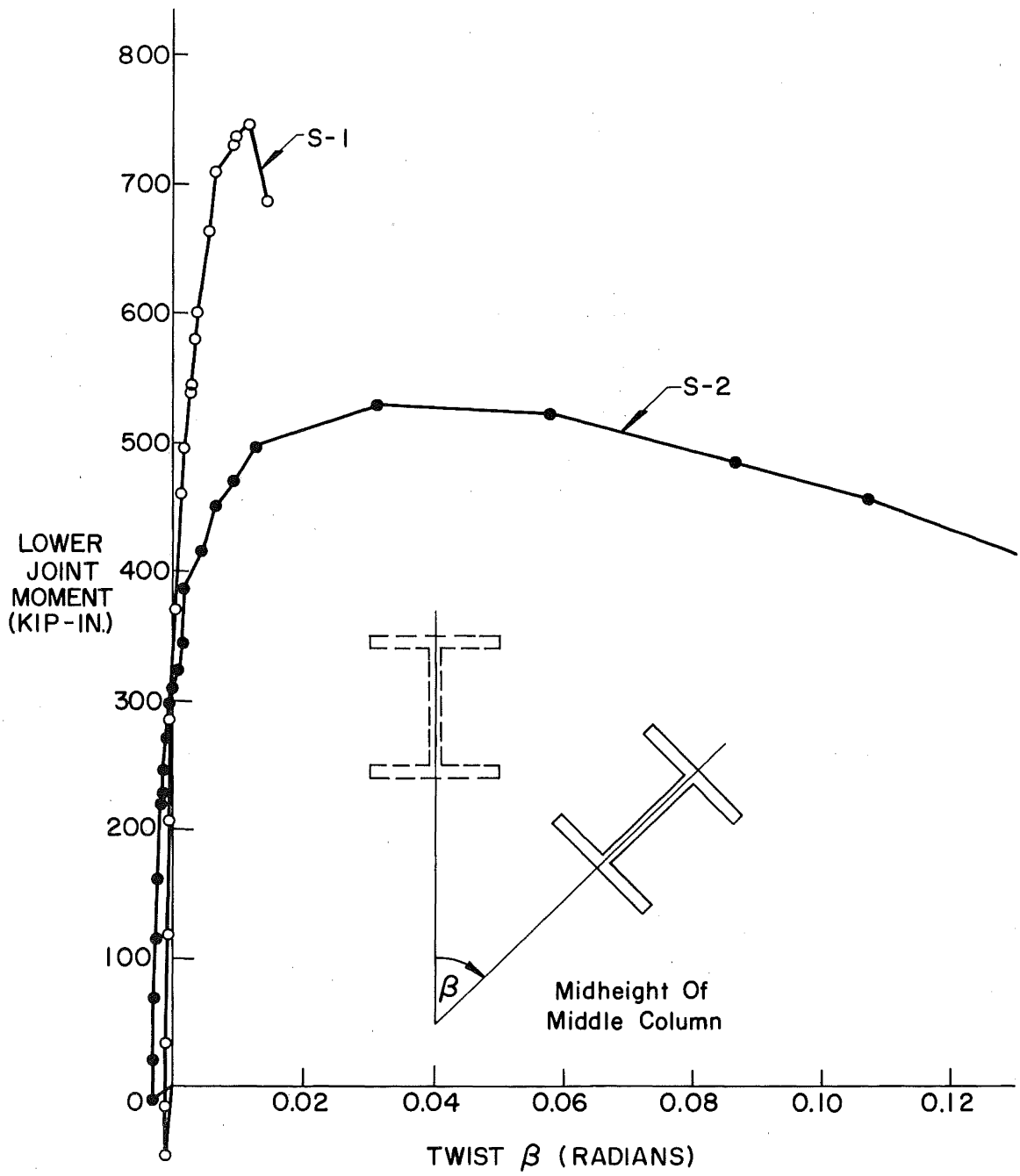
Fig. 17 Twist of Columns
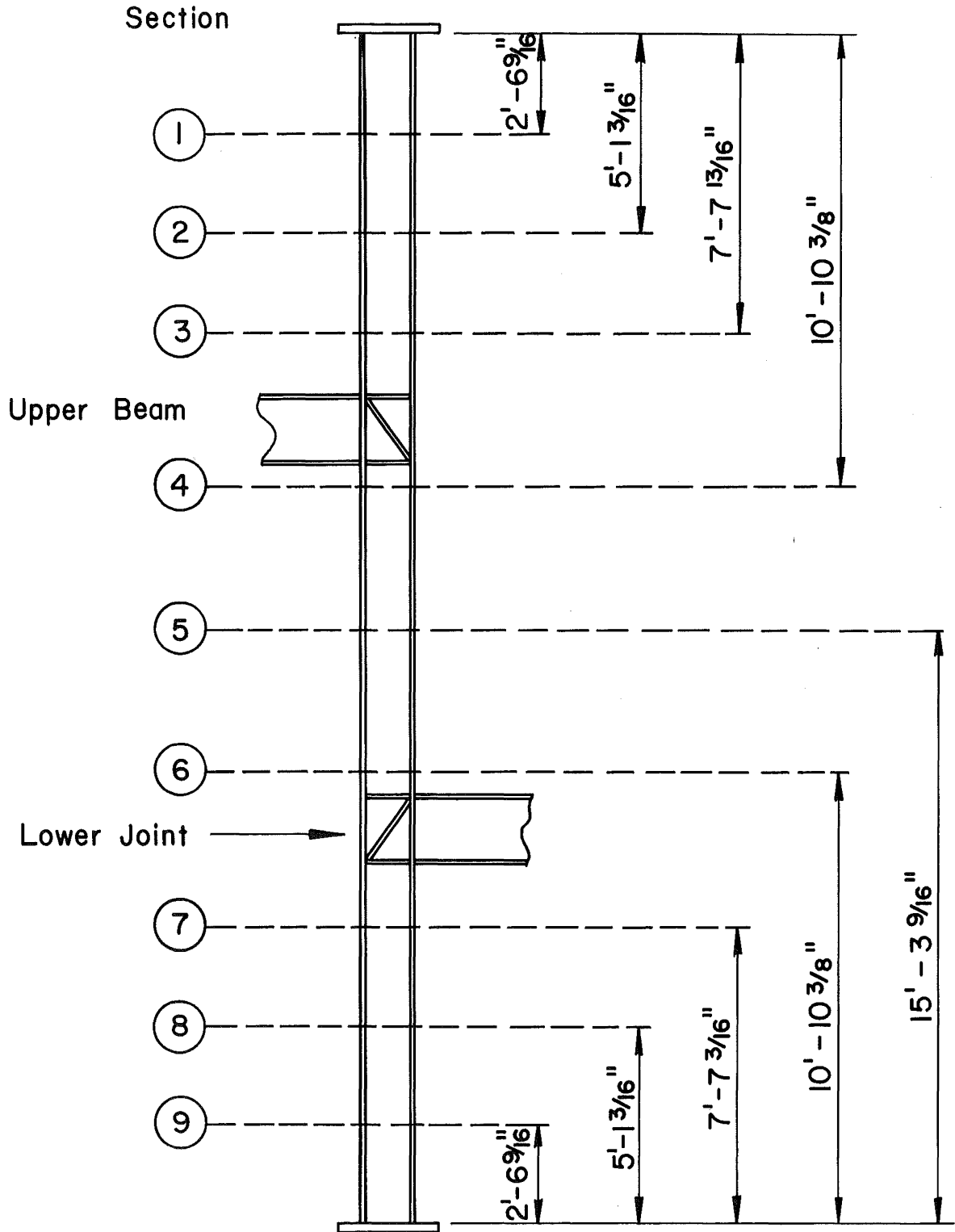
Fig. 18   Location of Sections at which Strains Due to Twisting were Recorded
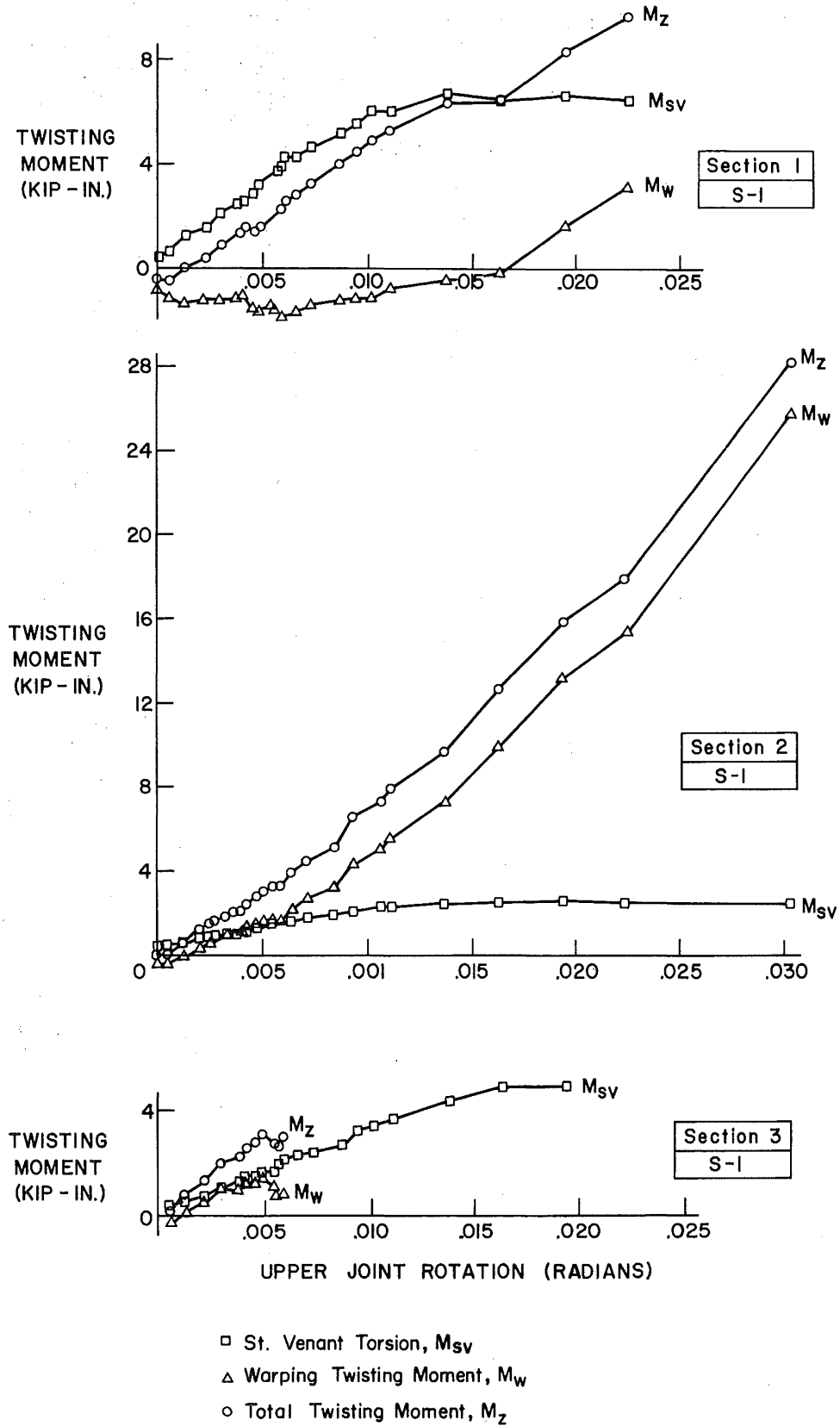
Fig. 19   Twisting Moment vs. Joint Rotation Relationships for
Upper Column of Subassemblage S-1
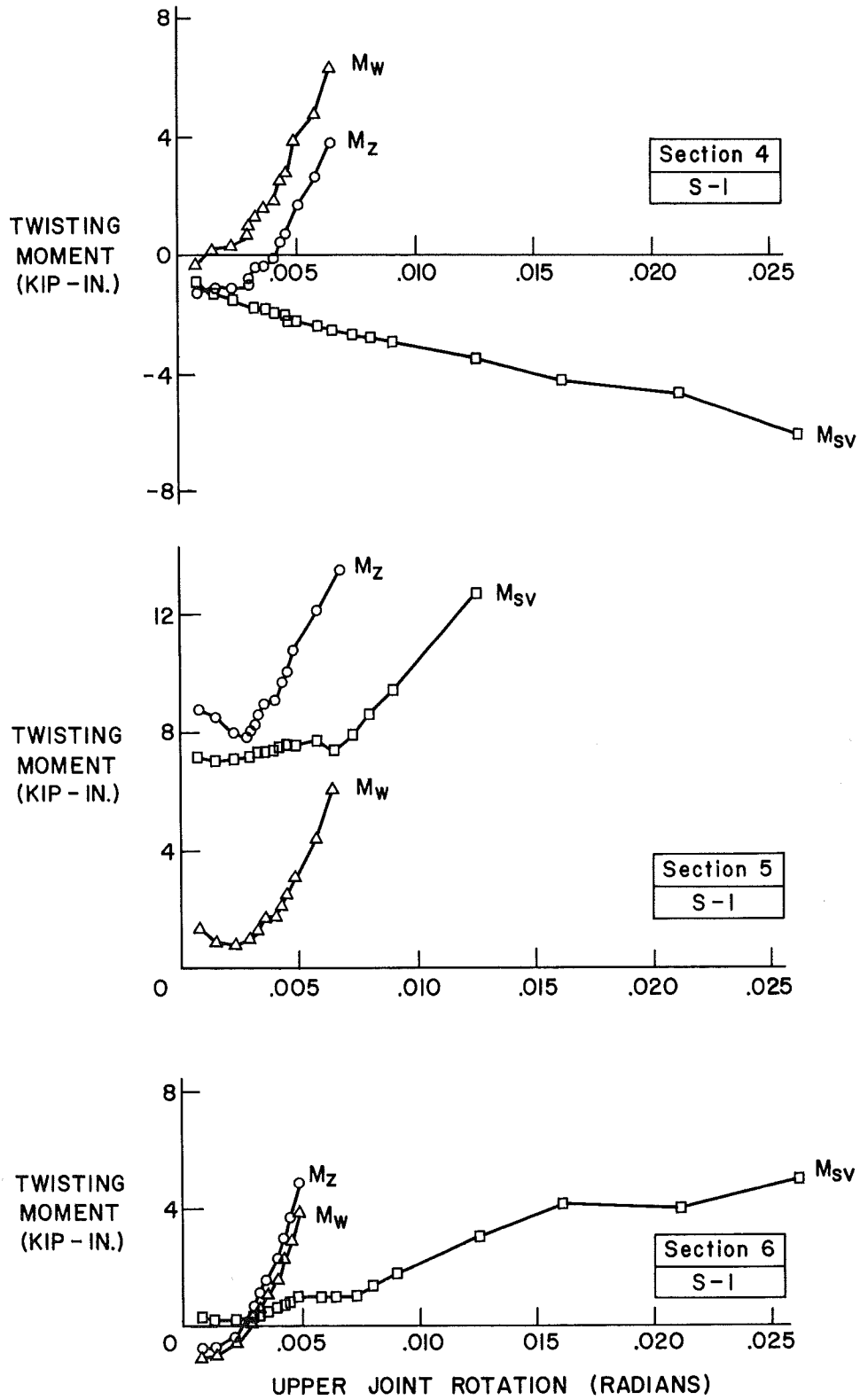
Fig. 20   Twisting Moment vs. Joint Rotation Relationships for
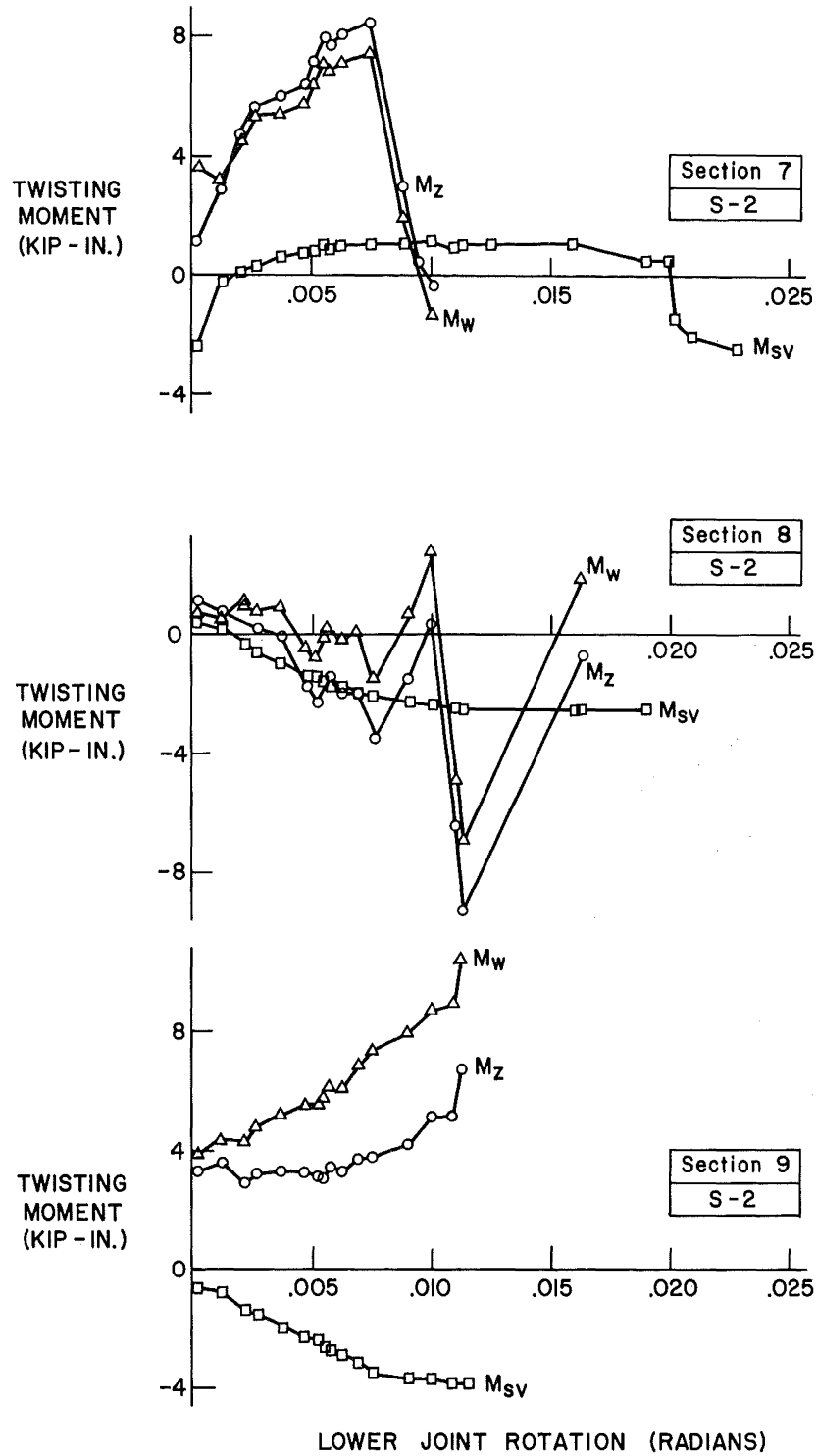Middle Column of Subassemblage S-1
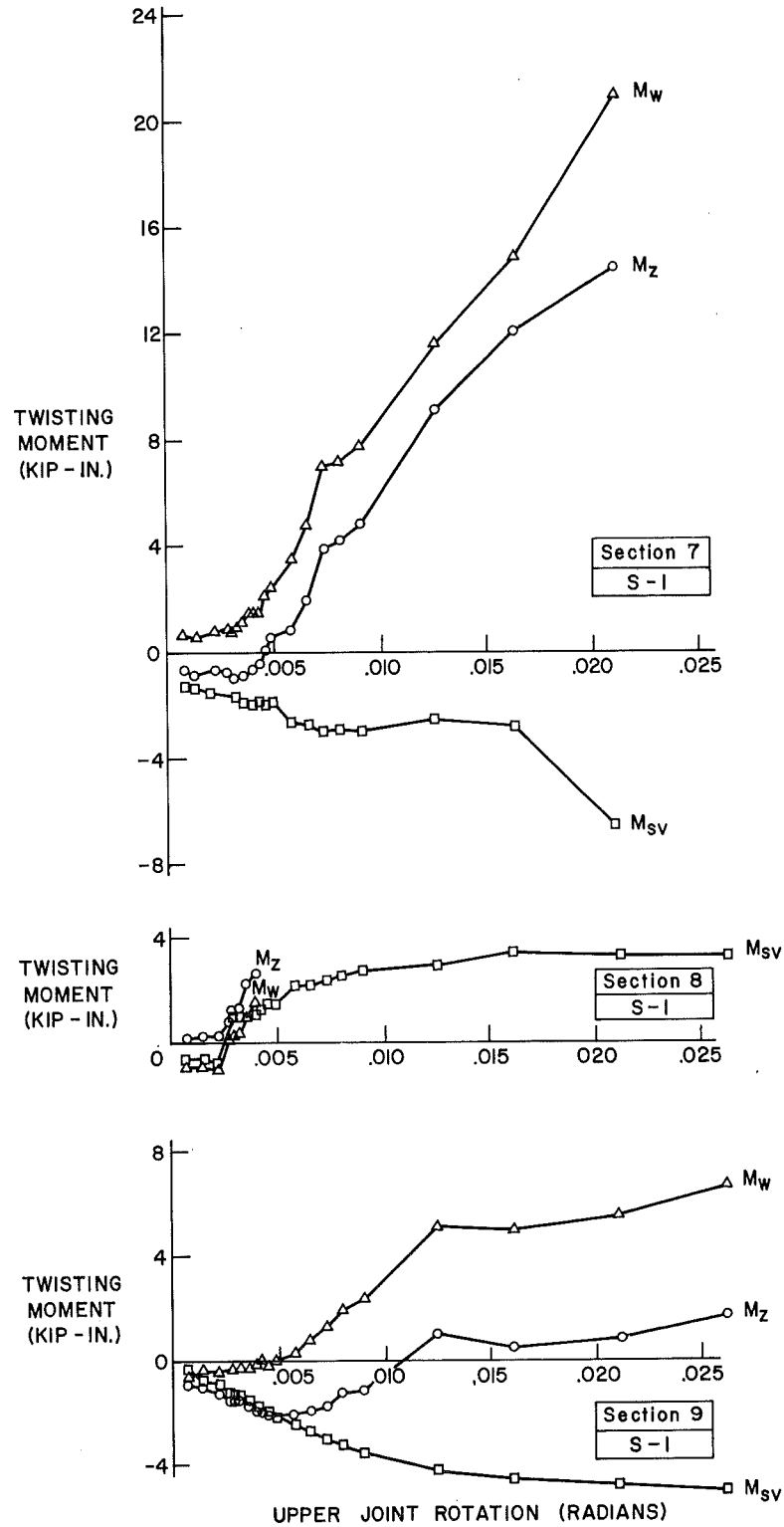
Fig. 21 Twisting Moment vs. Joint Rotation Relationships for
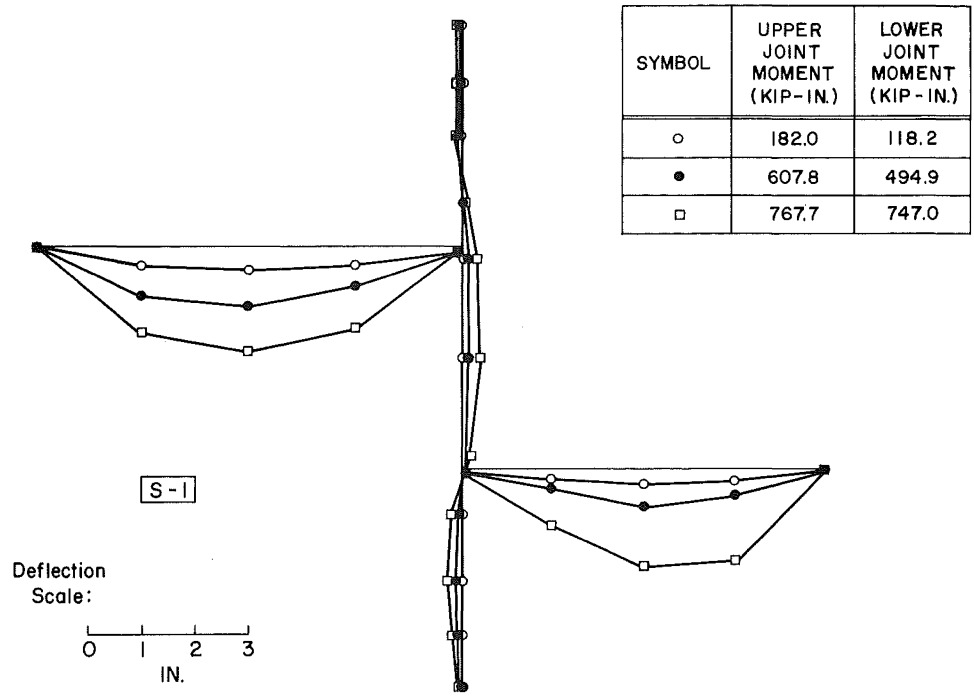Lower Column of Subassemblage S-1
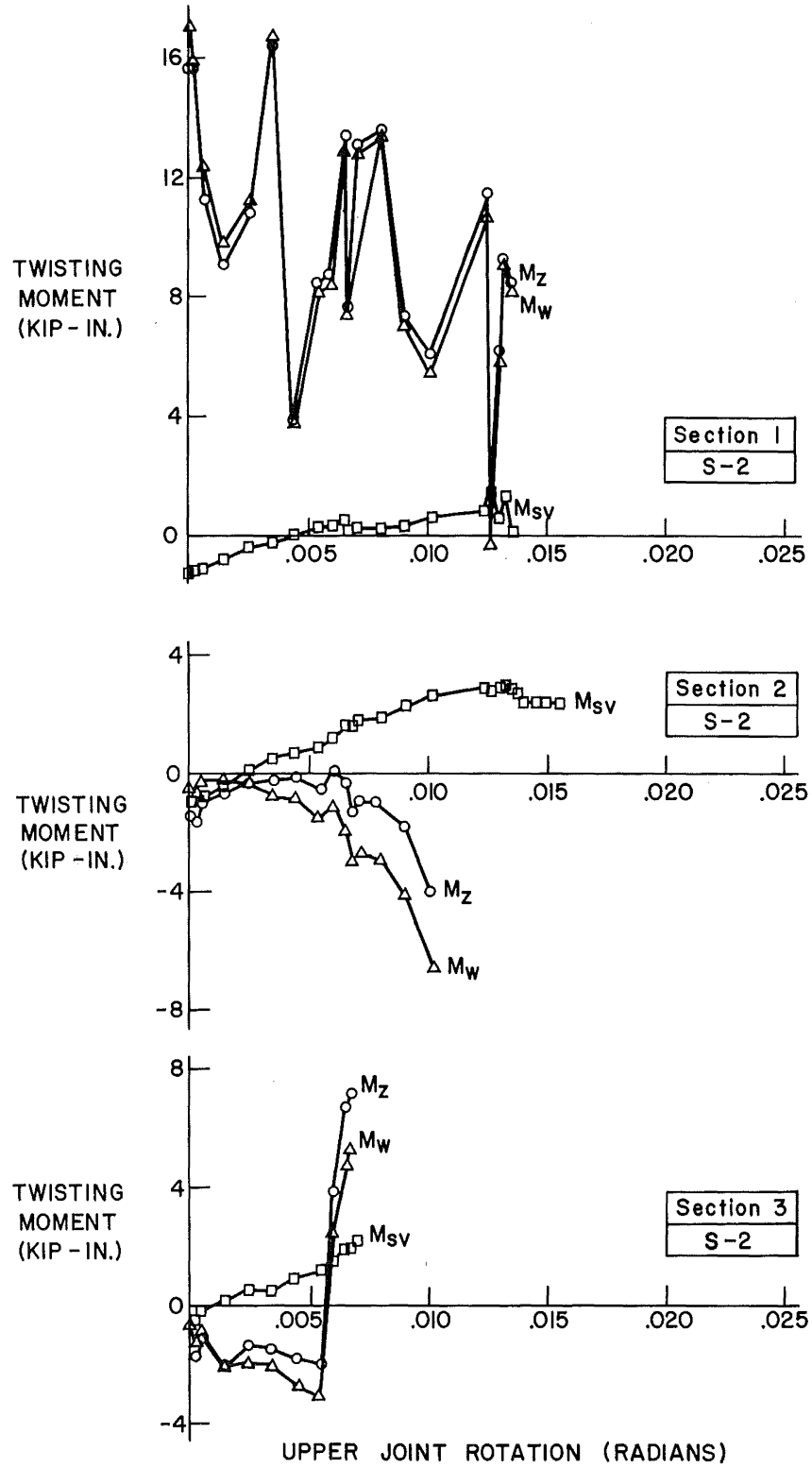
Fig. 22   Twisting Moment vs. Joint Rotation Relationships for
Upper Column of Subassemblage S-2
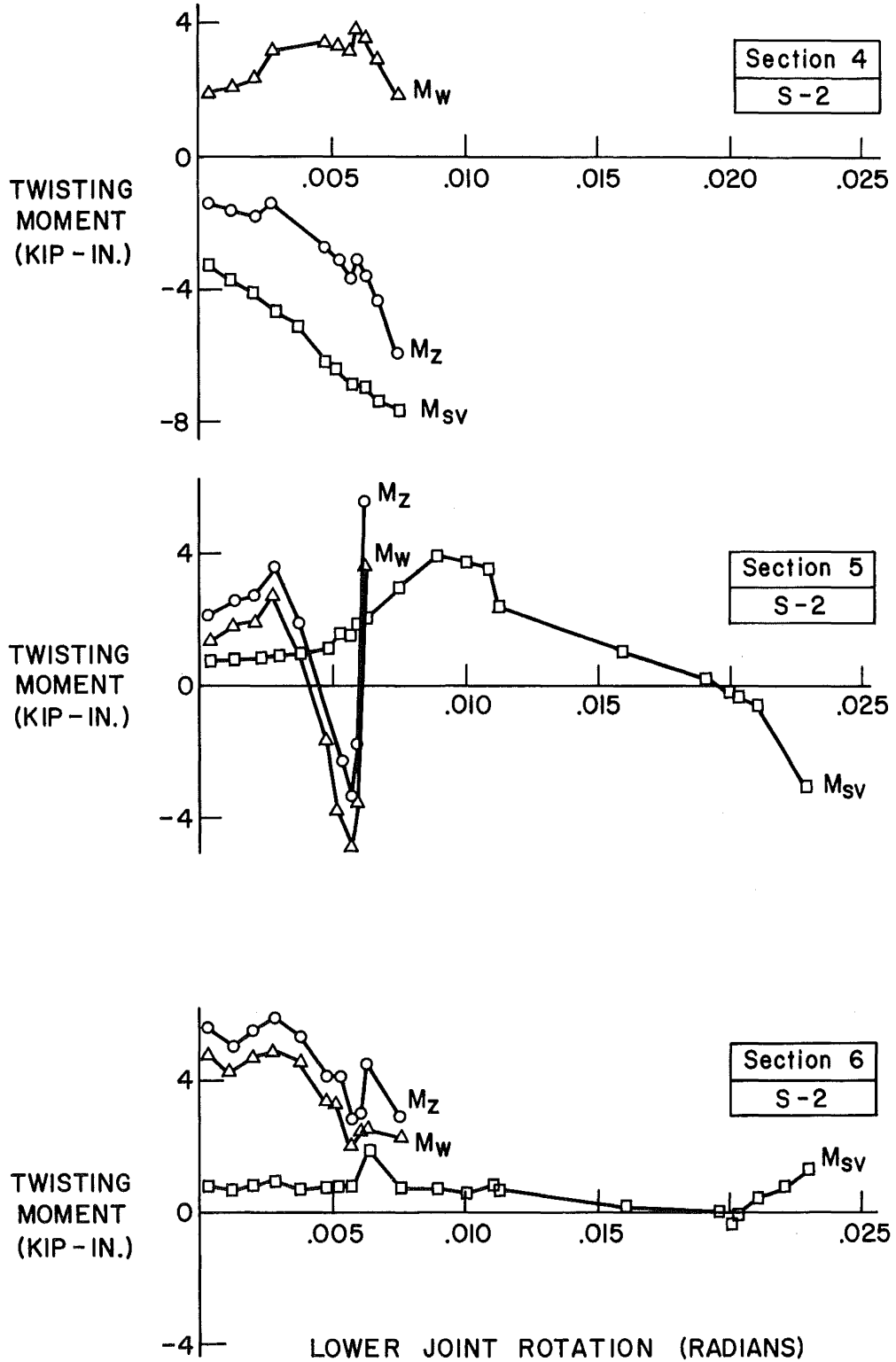
Fig. 23   Twisting Moment vs. Joint Rotation Relationships for
Middle Column of Subassemblage S-2

Fig. 24 Twisting Moment vs. Joint Rotation Relationships for
Lower Column of Subassemblage S-2

SYMBOL	UPPER JOINT MOMENT (KIP-IN.)	LOWER JOINT MOMENT (KIP-IN.)
○	182.0	118.2
●	607.8	494.9
□	767.7	747.0

S-1

Deflection Scale:

0 1 2 3
IN.

Fig. 25   In-Plane Deflection Profile of Subassemblage S-1
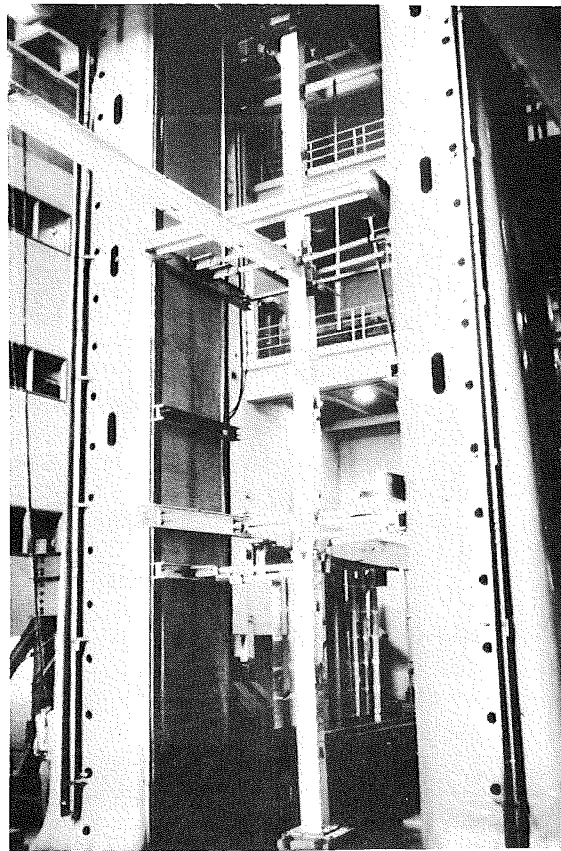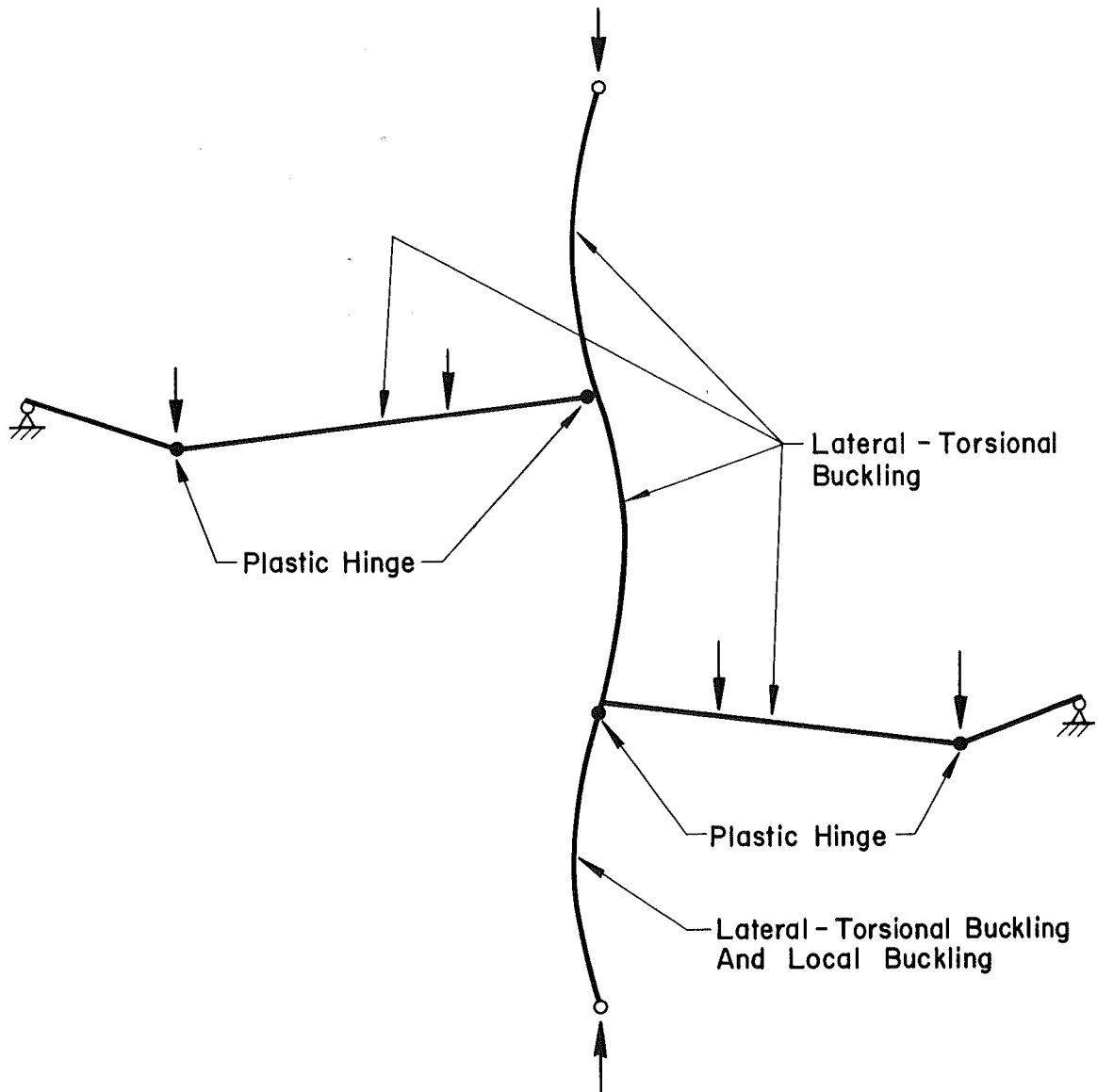

Fig. 26   Subassemblage S-1 After Test

Fig. 27 Modes of Failure for Subassemblage S-1

Fig. 28 Yielding in Column Below Lower Joint of Subassemblage S-1
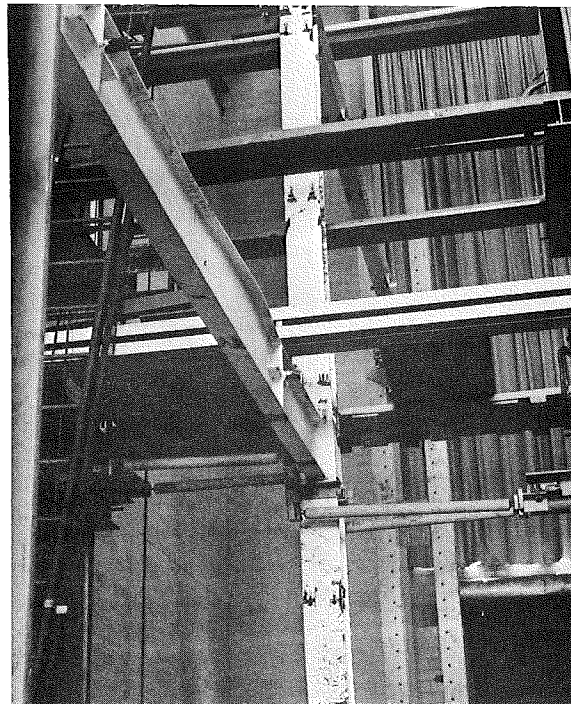

Fig. 29 Lateral-Torsional Deformation in Lower Column of Subassemblage S-1

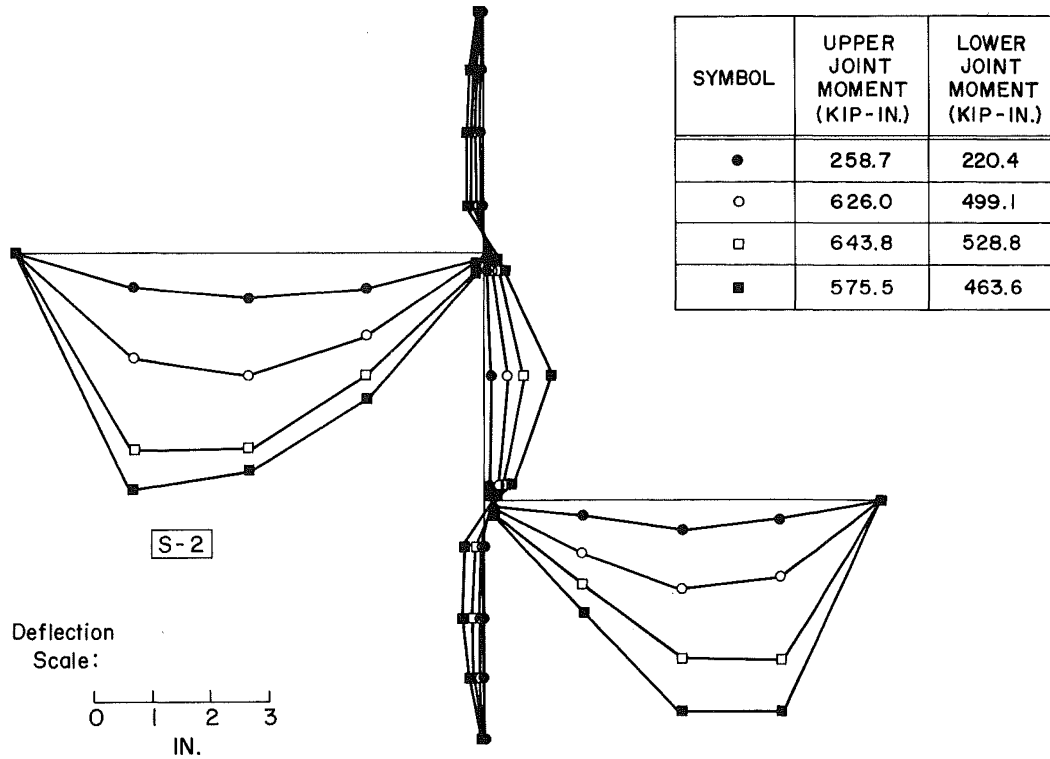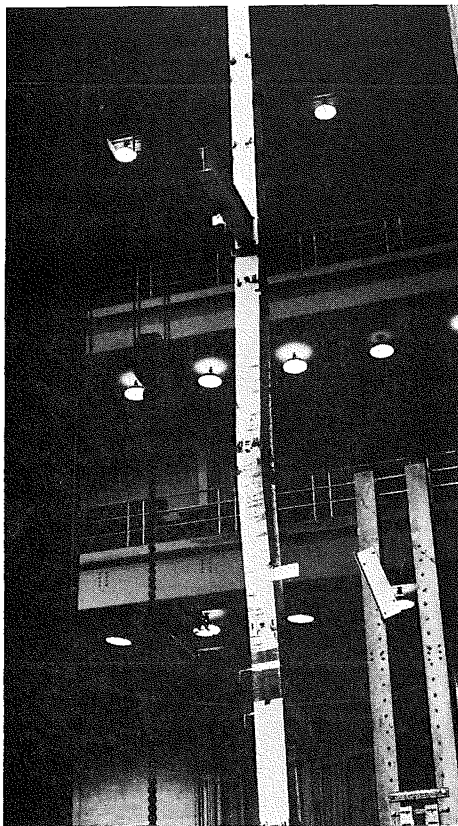| SYMBOL	UPPER JOINT MOMENT (KIP-IN.)	LOWER JOINT MOMENT (KIP-IN.)
●	258.7	220.4
○	626.0	499.1
□	643.8	528.8
▣	575.5	463.6

Fig. 30   In-Plane Profile of Subassemblage S-2

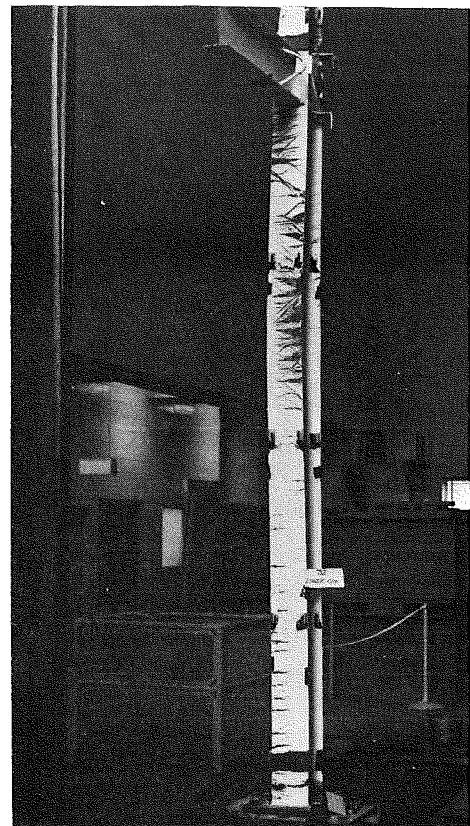Fig. 31   Middle Column of S-2 After Test

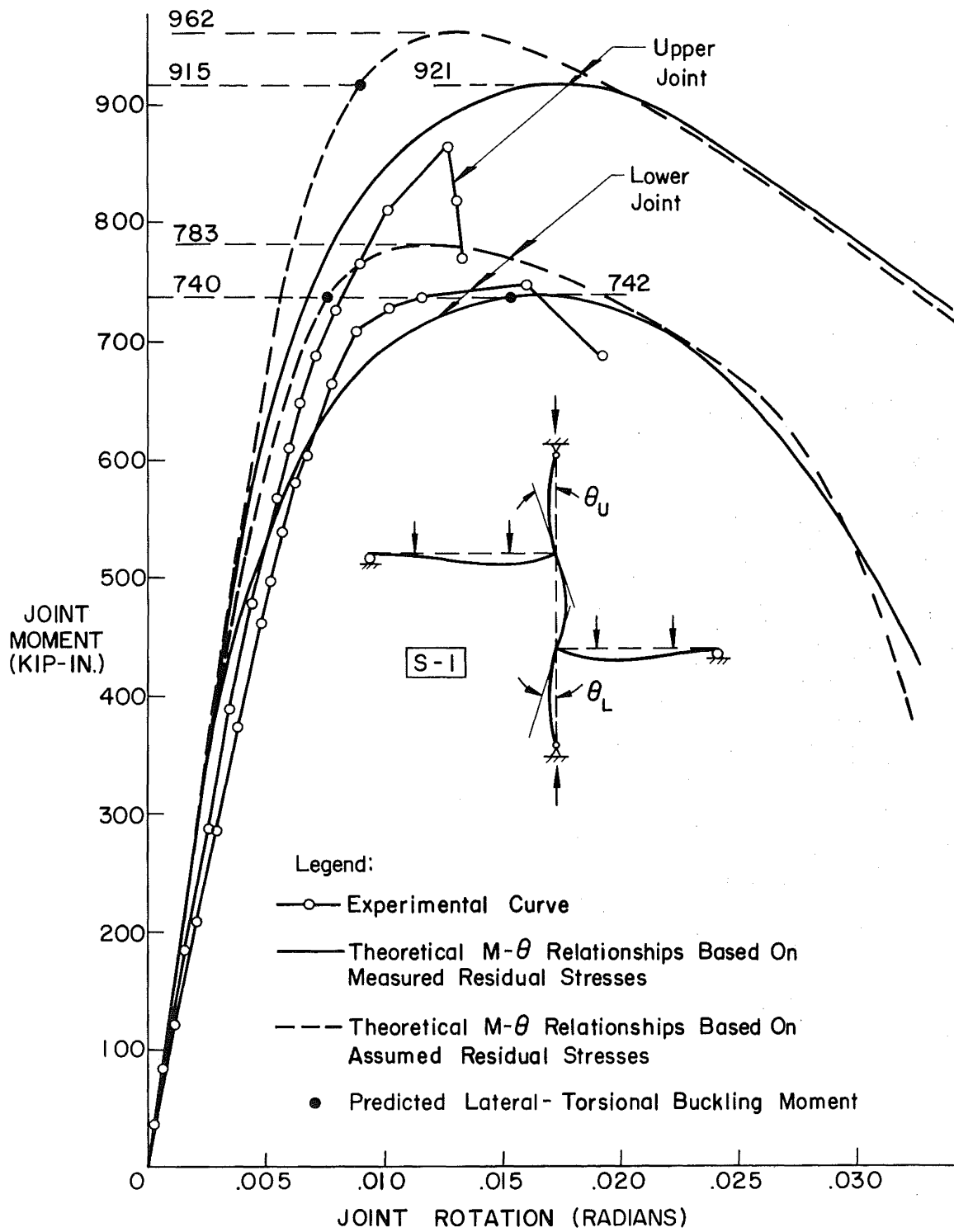Fig. 32   Lower Column of S-2 After Test

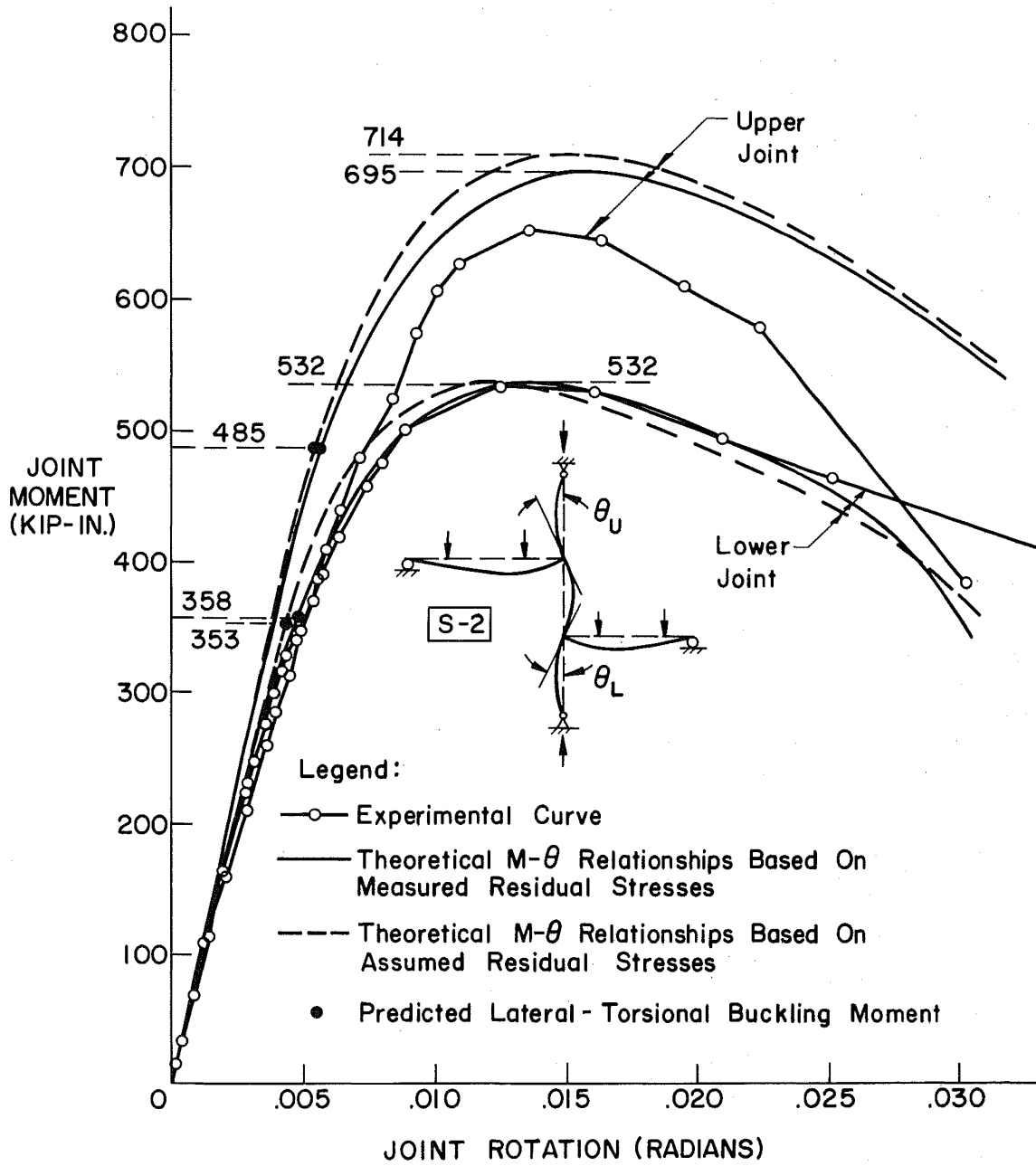Fig. 33 Moment-Rotation Relationships for Subassemblage S-1

Fig. 34   Moment-Rotation Relationships for Subassemblage S-2

10. REFERENCES

1. Driscoll, G. C., Jr. et al.
   PLASTIC DESIGN OF MULTI-STORY FRAMES - LECTURE NOTES AND
   DESIGN AIDS, Fritz Engineering Laboratory Report Nos.
   273.20 and 273.34, Lehigh University, August 1965.

2. AISI Committee
   PLASTIC DESIGN OF BRACED MULTI-STORY STEEL FRAMES, American
   Iron and Steel Institute, New York, 1968.

3. CRC
   GUIDE TO DESIGN CRITERIA FOR METAL COMPRESSION MEMBERS,
   Second edition, edited by B. G. Johnston, John Wiley and
   Sons, New York, 1966.

4. Campus, F. and Massonet, C.
   RECHERCHES SUR LE FLAMBEMENT DE COLONNES EN ACIER A37, A
   PROFIL EN DOUBLE TE SOLLICITEES OBLIQUEMENT, I.R.S.I.A.
   Comptes Rendus de Techerches, 17, April 1956.

5. Aglietti, R. A., Lay, M. G. and Galambos, T. V.
   TESTS ON A36 and A441 STEEL BEAM-COLUMNS, Fritz Engineering
   Laboratory Report No. 278.14, Lehigh University, June 1964.

6. Gent, A. R.
   ELASTIC PLASTIC COLUMN STABILITY AND THE DESIGN OF NON-
   SWAY FRAMES, Proceedings of the Institution of Civil
   Engineers, England, 34, p. 129, (June 1966).

7. Lim, L. C., Sheninger, E. L., Yoshida, K. and Lu, L. W.
   TECHNIQUES FOR TESTING STRUCTURAL SUBASSEMBLAGES WITH BRACED
   AND UNBRACED COLUMNS, Fritz Engineering Laboratory Report
   No. 329.2, Lehigh University, August 1969.

8. Lay, M. G. and Galambos, T. V.
   INELASTIC BEAMS UNDER MOMENT GRADIENT, Journal of the Struc-
   tural Division, ASCE, 93 (ST1), p. 381, (February 1967).

9. Lay, M. G. and Galambos, T. V.
   INELASTIC STEEL BEAMS UNDER UNIFORM MOMENT, Journal of the
   Structural Division, ASCE, 91 (ST6), p. 67, (December 1965).

10. Desai, S.
    TENSION TESTING PROCEDURE, Fritz Engineering Laboratory
    Report No. 237.44, Lehigh University, February 1969.

11. Huber, A. W.
    RESIDUAL STRAIN MEASUREMENT, Fritz Engineering Laboratory
    Report No. 220A.17, Lehigh University, March 1955.

12. Ojalvo, M.
      RESTRAINED COLUMNS, Proceedings of ASCE, 86 (EM5), p. 1,
      (October 1960).

13. Lim, L. C., Scheid, R. A. and Lu, L. W.
      COMPUTER PROGRAMS (FORTRAN IV) FOR M-P-$\emptyset$, CDC and M-θ
      RELATIONSHIPS FOR W BEAM-COLUMNS BENT ABOUT STRONG OR WEAK
      AXIS, Fritz Engineering Laboratory Report No. 329.4, Lehigh
      University, July 1970.

14. AISC
      STEEL CONSTRUCTION, Manual of American Institute of Steel
      Construction, sixth edition, 1963.

15. Lim, L. C., and Lu, L. W.
      THE STRENGTH AND BEHAVIOR OF LATERALLY UNSUPPORTED COLUMNS,
      Fritz Engineering Laboratory Report No. 329.5, Lehigh University,
      June 1970.